Quaternary Science Reviews 223 (2019) 105930

Contents lists available at ScienceDirect

Quaternary Science Reviews

journal homepage: www.elsevier.com/locate/quascirev

Holocene and Last Interglacial climate of the Faroe Islands from sedimentary plant wax hydrogen and carbon isotopes

Lorelei Curtin [a, b, *], William J. D'Andrea [a], Nicholas Balascio [c], Genevieve Pugsley [c], Gregory de Wet [d], Raymond Bradley [d]

[a] Lamont-Doherty Earth Observatory, Columbia University, 61 Route 9W, Palisades, NY, USA
[b] Department of Earth and Environmental Sciences, Columbia University, New York, NY, USA
[c] Department of Geology, The College of William & Mary, Williamsburg, VA, USA
[d] Department of Geosciences, University of Massachusetts, Amherst, MA, USA

ARTICLE INFO

Article history:
Received 19 May 2019
Received in revised form
30 August 2019
Accepted 9 September 2019
Available online 27 September 2019

Keywords:
Paleoclimatology
Holocene
Interglacial
North Atlantic
Organic geochemistry
Stable isotopes

ABSTRACT

The Last Interglacial period (LIG) is Earth's most recent globally warm period and is analogous in some ways to projected future global warming. However, questions remain regarding the state of the climate during the LIG in the North Atlantic, a region that is extremely sensitive to changes in oceanic and atmospheric circulation. Here, we present hydrogen and carbon isotope (δD and $\delta^{13}C$) records from a suite of plant wax biomarkers preserved in Holocene and LIG lacustrine sediments from the North Atlantic Faroe Islands and interpret them as qualitative proxies for temperature and hydroclimate variability. These data are used to directly compare LIG and Holocene climate using the same proxy approaches from the same terrestrial location. Measuring multiple isotopes on multiple types of waxes elucidates the sources of homologous plant waxes. We deduce that the δD values of long-chain *n*-alkanes (C_{27}–C_{33}) and mid-chain *n*-alkanes (C_{23}–C_{25}) in these sedimentary archives reflect leaf water and lake water δD values, respectively, while the δD values for both long-chain (C_{28}–C_{30}) and mid-chain n-alkanoic acids (C_{24}–C_{26}) primarily represent lake water δD values. Plant wax-inferred δD values of precipitation during the early Holocene (10,100 to 8,200 cal yr BP) are ~35‰ more positive than late Holocene values, and decline over the Holocene. δD-inferred hydrologic change and $\delta^{13}C$ -inferred plant water use efficiency both indicate that the Faroe Islands became drier throughout the Holocene. Comparison with measurements from LIG plant waxes indicates that late LIG in the Faroe Islands was hydrologically similar to the early-to mid-Holocene (8,200 to 4,000 cal yr BP), with enriched precipitation isotopes and reduced evapotranspiration indicating a warmer, wetter environment.

1. Introduction

To better understand how Earth's climate system will respond to anthropogenic warming, it is important to document climate patterns during warm periods of Earth's history. The Last Interglacial period (LIG; ~130 ka to 116 ka) was warmer than the preindustrial period in most regions (CAPE-Last Interglacial Project Members, 2006; Kukla et al., 2002; McKay et al., 2011; Otto-Bliesner et al., 2013; Turney and Jones, 2010), and is analogous in some ways to future warming scenarios. Climate reconstructions for the LIG have been developed using a variety of climate proxies from terrestrial and marine archives (Fig. 1) (Axford et al., 2009; Bauch et al., 1999; Björck et al., 2000; Cortijo et al., 1994; De Beaulieu and Reille, 1992; Kühl and Litt, 2003; Mangerud et al., 1981; McFarlin et al., 2018; Salonen et al., 2018; Shackleton et al., 2003; Zagwijn, 1996 and others). However, the magnitude of warming relative to modern temperature and the hydrological conditions of the terrestrial North Atlantic region during the Holocene and LIG have not been well documented.

Amplification of warming at high latitudes makes understanding the climatic conditions of the North Atlantic and Arctic during past warm periods particularly important (Holland and Bitz, 2003; Manabe and Stouffer, 1980; Serreze and Francis, 2006). Furthermore, deep water convection in the northern North Atlantic and Nordic Seas region is a critical component of the Atlantic

* Corresponding author. Lamont-Doherty Earth Observatory, 104 Geoscience, 61 Route 9W, Palisades, NY 10964, USA.
E-mail address: lcurtin@ldeo.columbia.edu (L. Curtin).

https://doi.org/10.1016/j.quascirev.2019.105930
0277-3791/

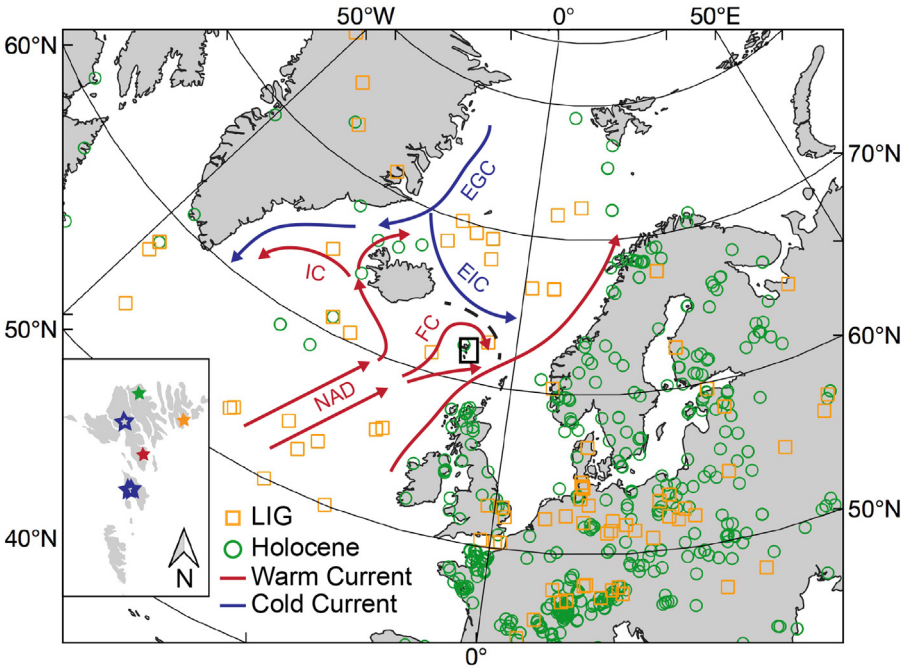

Fig. 1. Map of the North Atlantic region, marked with published full-Holocene (green circle) and LIG (yellow square) quantitative paleotemperature records (locations from Kaspar et al., 2005; Turney and Jones, 2010; Marcott et al., 2013; Sundqvist et al., 2014; Marsicek et al., 2018). Inset is the Faroe Islands, with a green star marking lake Eiðisvatn, yellow star marking the Klaksvík LIG section, red star marking the location of the instrumental climatological record, and blue stars marking the three locations where modern lake water isotope samples were collected. Red arrows and labels show warm surface ocean currents (NAD: North Atlantic Drift, FC: Faroes Current, IC: Irminger Current), while blue arrows and labels show cold surface currents (EGC: East Greenland Current, EIC: East Iceland Current). Black dashed line marks the Faroe-Iceland Front. (For interpretation of the references to color in this figure legend, the reader is referred to the Web version of this article.)

Meridional Overturning Circulation and oceanographic changes in the North Atlantic have been linked to abrupt climate changes globally (e.g. Younger Dryas, 8.2 ky event, Bond events, Dansgaard-Oeschger cycles) (Behl and Kennett, 1996; Broecker et al., 1990; Clark et al., 2002; Peterson et al., 2000; Wang et al., 2001). Most of our current understanding of LIG conditions in the North Atlantic region comes from marine sediment records, which do not document terrestrial climate. While terrestrial paleorecords from Europe suggest that LIG temperatures were 2–3 °C warmer than modern (Kaspar et al., 2005), records of sea surface temperatures are inconsistent regarding the difference in temperature between the LIG and Holocene. Some marine records show LIG temperatures up to 10 °C warmer than modern or preindustrial temperatures (Bauch et al., 1999; CLIMAP Project Members, 1984; Oppo et al., 2006), others suggest mean annual temperatures were as much as 2.6 °C cooler during the LIG (Bauch et al., 1999; CLIMAP Project Members, 1984), and still others indicate no difference at all (Cortijo et al., 1994). It is still unclear if the large differences in LIG temperature reconstructions are due to uncertainties in the climate proxies or actual regional differences in LIG temperatures. Modeling studies of LIG temperatures also yield conflicting results for the North Atlantic, with some showing up to 4–6 °C of warming relative to modern (McKay et al., 2011; Otto-Bliesner et al., 2013; Pfeiffer and Lohmann, 2016) while others suggest cooler temperatures or little to no difference (Gierz et al., 2017).

While most previous studies of the LIG have focused on marine records, terrestrial records of precipitation isotopes have the potential to reveal new information regarding atmospheric conditions during the LIG. Hydrogen and oxygen isotope values (δD and $\delta^{18}O$) of precipitation vary spatially across Earth's surface and reflect atmospheric circulation patterns and other aspects of Earth's climate and hydrological cycle. In the North Atlantic, precipitation isotopes are anomalously enriched in deuterium (D) and ^{18}O for their latitude, due to the northeastward transport of heat and moisture into the region by oceanic and atmospheric circulation (Bowen and Revenaugh, 2003). Therefore, times of reduced ocean heat transport and atmospheric heat and moisture transport to the northern North Atlantic from southwesterly sources are characterized more negative isotopic values of precipitation. For example, a modeling study of the 8.2 ky cooling event suggests that the isotopes in precipitation across in this region would have become more negative during cold periods with reduced meridional overturning circulation (LeGrande and Schmidt, 2008). It follows that during past warm intervals, such as the LIG and the early Holocene, the isotopic composition of precipitation would have been more positive; however, this has not been well documented across the North Atlantic region.

The Faroe Islands are located between Iceland and Scotland, where the climate is strongly influenced by the magnitude of ocean and atmospheric heat and moisture transport into the northern North Atlantic and the Nordic Seas. Because precipitation isotopes in the North Atlantic region are not only sensitive to local changes in temperature, but more broadly reflect regional ocean and atmospheric circulation patterns, records of past precipitation isotopes from terrestrial sediment archives on the Faroe Islands document past changes in regional climate and oceanographic conditions. While lakes containing Holocene-length sedimentary records are ubiquitous in the North Atlantic region, terrestrial LIG sedimentary archives are rare because the region was extensively glaciated during the last glacial period. On the Faroe Islands a LIG-aged lacustrine sedimentary unit survived the last glaciation and provides an archive of LIG climate information (Bennike et al., 2018; Geikie, 1881; Wastegård et al., 2005). Thus, LIG climate conditions in the Faroes can be directly compared to Holocene climate by reconstructing precipitation isotopes from both Holocene and LIG lake sediments.

Past precipitation isotopes can be reconstructed using the δD value of hydrogen contained in plant wax molecules, which are well preserved in lake sediments. The hydrogen isotope composition of plant waxes reflects the isotopic composition of the plant's source water, after modification due to biosynthetic fractionation and evaporative enrichment (Kahmen et al., 2013; Sachse et al., 2012, 2004; Sauer et al., 2001). Plant waxes are deposited and preserved in lake sediment and can therefore be used to reconstruct the isotopic composition of their source water through time (Sachse et al., 2012). The hydrogen isotope fractionation between source water and plant wax can vary between plant types, species, and individuals (Chikaraishi et al., 2004; Chikaraishi and Naraoka, 2007; Diefendorf et al., 2011; Zhang and Sachs, 2007), and therefore large shifts in vegetation within the watershed can affect a sedimentary plant wax hydrogen isotope record (Feakins, 2013). Despite such potentially confounding factors, the strong relationship between δD values of plant waxes and δD values of precipitation has been demonstrated in studies from across the world (Hou et al., 2008; Polissar and Freeman, 2010; Sachse et al., 2012, 2004 and references therein).

Here, we present Holocene and LIG records of plant wax hydrogen and carbon isotopes ($\delta^{13}C$) from the Faroe Islands, which we use to infer past changes in precipitation isotopes and hydroclimate. The objectives of this study are to document the Holocene evolution of climate in the Faroe Islands, and to compare the Holocene to late-LIG climate using the same paleoclimate proxies. The Holocene record we present is derived from lake sediments from Eiðisvatn and the LIG record from an exposure of lacustrine sediment near Klaksvík on Borðoy (Fig. 1). We report results from multiple plant wax types (*n*-alkanes and *n*-alkanoic acids), chain lengths, and isotope systems (δD and $\delta^{13}C$) to evaluate the sources of plant waxes and the environmental signals reflected by the sedimentary plant wax δD from these locations. We use $\delta^{13}C$ measurements to constrain the provenance of the leaf waxes and as an independent means of understanding changes in hydrologic conditions through changes in water use efficiency of plants. Faroe Island precipitation isotopes during the late LIG were very similar to those of the early to mid-Holocene, and both were enriched in deuterium relative to preindustrial values. We conclude that regional ocean and atmospheric conditions in the late LIG were similar to those in the early to mid-Holocene.

2. Study area

2.1. Background

The Faroe Islands are an archipelago of 18 islands located between Iceland and Scotland and between the Norwegian Sea and the North Atlantic (62°N, 7°W; Fig. 1). The islands are the remnants of a Tertiary flood basalt platform that erupted during the opening of the North Atlantic Basin (Rasmussen and Noe-Nygaard, 1970). The climate of the Faroes is strongly connected to local oceanographic conditions. The archipelago is located in the main pathway of the warm northward flowing North Atlantic Drift, and the cold East Iceland current approaches the Faroes from the northwest (Fig. 1). The boundary between cold and warm currents, the Iceland-Faroe Front, is located to the north of the Faroe Islands. Winters are mild and summers are cool (Fig. 2), and the precipitation is largely sourced from storms that approach from the southwest (Cappelen, 2018). Annual precipitation amounts vary from 1000 mm/yr at lower elevations to 3000 mm/yr at high elevations in the northwest (Cappelen, 2018).

The closest Global Network of Isotopes in Precipitation (GNIP) station to the Faroe Islands is in Reykjavík, Iceland approximately 800 km away. Climate conditions in Reykjavík are similar to those

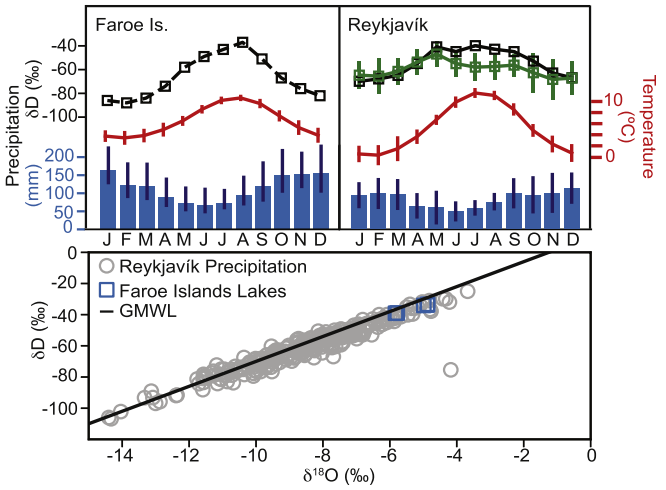

Fig. 2. Top panels: Faroe Islands and Reykjavík climatology and precipitation isotopes. Reykjavík climatology and precipitation isotopes are from the Global Network of Isotopes in Precipitation database, which includes monthly average amount-weighted precipitation isotopes (green squares with one standard deviation error bars), temperatures (red line with one standard deviation error bars), and precipitation amounts (blue bars with one standard deviation error bars) from 1960 to 2018. Faroe Islands climatology is from published technical reports from the Danish Meterological Institute (Cappelen, 2018), which includes monthly average temperature (red line with one standard deviation error bars) and precipitation amounts (blue bars with one standard deviation error bars) from 1992 to 2018 in Tórshavn. Black squares in both top panels indicate OIPC modeled precipitation isotopes. Bottom panel: grey circles indicate δD and $\delta^{18}O$ values of all precipitation samples from Reykjavik from GNIP. Blue squares indicate δD and $\delta^{18}O$ values of water samples from Faroese lakes collected in August of 2015. Black line indicates the GMWL. (For interpretation of the references to color in this figure legend, the reader is referred to the Web version of this article.)

in the Faroes (Fig. 2), and precipitation δD values at Reykjavik have a seasonal range of ~20‰. The Online Isotopes in Precipitation Calculator suggests an even larger seasonal range of ~50‰ in the Faroe Islands (Bowen, 2019) based on interpolation of existing precipitation isotope data (Bowen et al., 2005). However, the OIPC overestimates the seasonal range in the isotopes of precipitation for Reykjavík compared to the GNIP measurements (Fig. 2), so it is possible that the seasonal range modeled for the Faroe Islands is similarly overestimated. The North Atlantic Oscillation (NAO) is the dominant mode of inter-annual atmospheric variability in the North Atlantic region and is strongly correlated with precipitation isotopes in central Europe and in the North Atlantic high latitudes, however, no correlation has been found between the NAO and the isotopes of precipitation in the Faroe Islands (Baldini et al., 2008).

The Faroes were covered by a local ice cap during the last glacial period (Jørgensen and Rasmussen, 1986). Basal dates from lake sediment cores indicate that deglaciation occurred ~11,700–12,100 cal yr BP (Andresen et al., 2006; Olsen et al., 2010), probably coincident with the end of the Younger Dryas cold period. The sediments that have accumulated in Faroese lakes since the local deglaciation provide high-resolution archives of paleoenvironmental conditions throughout the Holocene. A general understanding of Holocene environmental history in the Faroes has been gained through various palynological and geochemical studies of lake sediments across the archipelago (Hannon et al., 2010, 2003; 2001, 1998; Jessen et al., 2008; Johansen, 1985, 1981; 1975; Lawson et al., 2005, 2008; 2007; Olsen et al., 2010). Human settlement of the Faroes occurred late in the Holocene (within the last ~2000 years), and so unlike most European sites, the Holocene records are largely undisturbed by human activities. Most archaeological evidence points to settlement by the Norse in the 9th century A.D. (Arge et al., 2005; Hannon et al., 2001), although there is some

palynological and archaeological evidence that suggests earlier settlement (Hannon et al., 2005, 2001; Hannon and Bradshaw, 2000; Johansen, 1985; Church et al., 2013).

2.2. Study sites

Eiðisvatn is located on the northern end of the island of Eysturoy at 62°17′10.3″N, 7°03′27.4″W. The lake has a surface elevation of 129 m above sea level and had a surface area of 0.47 km^2 prior to construction of a hydroelectric dam in the late 1980s, which expanded the lake area. Several small inlets flow into the lake, and tunnels bring water from neighboring valleys into the lake today. Before the lake was dammed, there was one major outlet stream. Eiðisvatn, like other hydrologically open lakes on the Faroes, likely has lake water isotope values that are very similar to precipitation (Fig. 2).

An organic-rich sediment deposit laying between two glacial till deposits is located at 62°13′25.2″N, 6°34′22.2″W in a coastal cliff section near Klaksvík, on Borðoy in the Faroe Islands (Geikie, 1881). The section is approximately 1 m thick, and is composed of silt and clay (Bennike et al., 2018). Total organic content of the sediment decreases from ~6% near the bottom to 2% at the top (Wastegård et al., 2005). Radiocarbon analyses of pieces of wood found in the unit yielded infinite ages (Rasmussen, 1972), and the deposit has since been stratigraphically assigned as late LIG via the occurrence of the 5e-Midt/RHY tephra throughout the section (Wastegård et al., 2005). Macrofossil, sedimentological and diatom analyses all indicate that the sequence represents a lacustrine environment with occasional marine overwash deposits (Bennike et al., 2018; Wastegård et al., 2005).

3. Methods

3.1. Chronology and loss on ignition

Two gravity cores, EI-D-01-15 (73.7 cm) and EI-D-02-15 (100.7 cm) were collected from the lake to preserve the sediment-water interface. The top 10 cm of EI-D-01-15 were extruded and subsampled in the field. A 2.82 m piston core, EI-P-01-15, was also collected using a percussion coring device. 17 terrestrial plant macrofossils and 4 bulk sediment samples were collected from the two surface cores and the piston core for AMS ^{14}C measurements. Samples were treated with a base-acid-base sequence to remove carbonate and humic contamination, combusted, and graphitized for measurement at either the UC-Irvine W. M. Keck Carbon Cycle AMS Laboratory or at the Woods Hole NOSAMS Laboratory.

Sediment samples (1 cm^3) from three visible tephra layers in the core were digested in 10% H_2O_2 to remove organic matter, washed over a 63 μm sieve using deionized water, and subjected to heavy-liquid density separations to isolate material with densities of 2.3–2.5 g/cm^3 (Blockley et al., 2005; Turney et al., 1997). Samples were then mounted on glass slides in epoxy resin, examined using light microscopy, and polished to expose grain interiors. Major oxide geochemical compositions were determined using wavelength-dispersive spectroscopy on an ARL-SEMQ electron microprobe equipped with six wavelength-dispersive spectrometers and a Bruker 5030 SDD energy-dispersive spectrometer at the Concord University Microanalytical Laboratory (WV, USA) using a 6 μm beam diameter, 14 kV accelerating voltage, and 10 nA beam current. Reported data are non-normalized oxide concentrations with each datum representing a single analysis of one tephra grain. Glass shard compositions were compared to previously described tephra horizons from the Faroe Islands (as reviewed by Wastegård et al., 2018).

Twenty-one radiocarbon and the three identified tephras were used to build an age model for the Holocene sediment using the Bayesian framework calibration software code 'Bacon' in R (Blaauw and Christen, 2011), using the IntCal13 calibration curve (Reimer et al., 2013). Eight radiocarbon samples were found to have anomalously old ages and were excluded from the final age model.

Weight loss-on-ignition (LOI) was measured on 1 cm^3 subsamples at 1 cm intervals in EI-D-02-15 and EI-P-01-15 following Heiri et al. (2001). Gravity and piston cores were aligned on a composite depth scale by aligning wt. % LOI measurements.

3.2. Organic and stable isotope geochemistry

1 cm-thick samples were taken from the piston core every 10 cm, along with the top 1 cm of each of the gravity cores, for lipid biomarker analysis. Samples were freeze-dried and then homogenized using a ceramic mortar and pestle. Lipids were extracted from the sediment samples using a Dionex Accelerated Solvent Extractor with a 9:1 solution of dichloromethane (DCM) and methanol. Each sample was subjected to three 5-min extraction cycles at 100 °C and 1000 psi.

Compounds in the total lipid extract were separated using silica gel flash column chromatography over 0.75 g of solvent-rinsed 100% activated silica gel. Aliphatic, ketone, and polar fractions were separated by successive elution with 4 ml of hexane, DCM, and methanol, respectively. Solid-phase aminopropyl column chromatography was used to isolate n-alkanoic acids from the polar fraction, by successive elution with 4 mL of 2:1 DCM:isopropanol and 4% acetic acid in diethyl ether. The second fraction, which contained the n-alkanoic acids, was methylated overnight at 50 °C using 2% HCl in methanol to form n-alkanoic acid methyl esters for analysis. The straight chain n-alkanoic acid methyl esters were separated from hydroxyl acid esters and other polyfunctional compounds using silica gel flash column chromatography with 4 ml of hexane and DCM as eluents. The DCM fraction containing the *n*-alkanoic acid methyl esters, and the original hexane fraction from the first silica gel separation containing n-alkanes, were dried under N_2 gas and reconstituted in 100 μL of hexane for analysis.

n-Alkanes and *n*-alkanoic acids were identified and quantified using an Agilent 7890 A gas chromatograph equipped with a mass selective detector (MSD) and a flame ionization detector (FID) using a 30 m-long DB-5 capillary column with an internal diameter of 250 μm. Initial GC oven temperature was set to 60 °C, then ramped to 150 °C at 15 °C per minute, and then ramped to 320 °C at 4 °C per minute. Compounds were identified by comparison of the mass spectra and retention times to an *n*-alkane standard containing C_{10}–C_{40} *n*-alkanes (Sigma Aldrich Supelco 40147-u) and an *n*-alkanoic acid standard solution containing the even *n*-alkanoic acids from C_8–C_{32} (Nu-Chek prep mixture 19 A and Larodan mixture Me 277). The external standards were used to determine compound-specific FID peak area response factors and to quantify compounds of interest in each sample.

δD and $\delta^{13}C$ values of *n*-alkanes and n-alkanoic acids were measured via GC-IRMS on a Thermo Trace GC coupled to a Thermo Delta V through an Isolink Conflo IV. Sample D/H and $^{13}C/^{12}C$ measurements were referenced to the VSMOW and VPDB scales, respectively, according to the recommendations of Polissar and D'Andrea (2014) and using Mix A5 and Mix A7 standards with 15 *n*-alkane molecules whose D/H and $^{13}C/^{12}C$ were determined off-line by Arndt Schimmelmann at the University of Indiana. All sample isotope ratios are reported using standard δ notation,

$$\delta D,\ \delta^{13}C = \left(\frac{R_{sample}}{R_{VSMOW,\ \ VPDB}} - 1\right) \times\ 1000. \quad (1)$$

where R = D/H or $^{13}C/^{12}C$. *n*-Alkanoic acid δD and $\delta^{13}C$ values were mathematically corrected for methyl group addition by analyzing the δD and $\delta^{13}C$ of a sample of phthalic acid that was methylated alongside sample *n*-alkanoic acids. Results were processed and pooled analytical uncertainties (1 s.e.m.) in sample δD and $\delta^{13}C$ values were calculated and reported according to Polissar and D'Andrea (2014).

3.3. Biomarker indices

Average chain lengths (ACL) of *n*-alkanes and *n*-alkanoic acids were calculated using the formula

$$ACL_{alk,\ acid} = \frac{\sum (C_i)(X_i)}{\sum C_i} \quad (2)$$

where C_i is the concentration of a given *n*-alkane or *n*-alkanoic acid relative to total alkane or n-alkanoic acid concentration, X_i is the carbon chain length, and i = odd numbers from 21 to 35 for *n*-alkanes and even numbers from 20 to 34 for *n*-alkanoic acids (Poynter and Eglinton, 1990).

Deuterium fractionation between terrestrially-sourced *n*-alkanes (C_{29}, C_{31}, and C_{33}) and aquatically-sourced *n*-alkanes (C_{25} and C_{27}) ($\varepsilon_{2Hterr\text{-}2Haq}$) was calculated using standard epsilon notation:

$$\varepsilon_{2Hterr-2Haq} = 1000\left[\frac{(\delta D_{terr} + 1000)}{(\delta D_{aq} + 1000)} - 1\right]. \quad (3)$$

n-Alkanes were designated terrestrial vs. aquatic based on the trends in δD values and the carbon isotope values (discussed in section 5.1). Carbon fractionation between *n*-alkanes and their biosynthetically equivalent *n*-alkanoic acids ($\varepsilon_{13Calk\text{-}13Cacid}$) are also expressed in standard epsilon notation, such that:

$$\varepsilon_{13Calk-13Cacid} = 1000\left[\frac{\left(\delta^{13}C_{n-alkane} + 1000\right)}{\left(\delta^{13}C_{n-alkanoic\ acid} + 1000\right)} - 1\right]. \quad (4)$$

Intrinsic water use efficiency (iWUE), defined as the amount of carbon assimilated per water transpired, can be calculated according to the following equation (Ehleringer et al., 1993; Feng, 1999):

$$iWUE = \frac{c_a - c_i}{1.6}, \quad (5)$$

where c_a is the concentration of CO_2 outside a leaf and c_i is the concentration of CO_2 in the leaf intercellular space. C_i values can be calculated according to the following equation:

$$1000\left[\frac{\left(\delta^{13}C_{atm} + 1000\right)}{\left(\delta^{13}C_{plant} + 1000\right)} - 1\right] = a + (b - a)\frac{c_i}{c_a}, \quad (6)$$

where $\delta^{13}C_{atm}$ is the $\delta^{13}C$ value of atmospheric CO_2, $\delta^{13}C_{plant}$ is the $\delta^{13}C$ value of bulk plant material, a is the fractionation associated with gas diffusion into the leaf (~-4.4‰), and b is the fractionation associated with the Rubisco enzyme during carboxylation (~-27‰). The apparent fractionation between bulk plant and *n*-alkanes is approximately 6‰ (Chikaraishi and Naraoka, 2001; Collister et al., 1994). Using pCO_2 and $\delta^{13}C_{atm}$ values from ice cores (Elsig et al., 2009; Lourantou et al., 2010; Monnin et al., 2004), c_i and iWUE can be calculated from $\delta^{13}C$ values of terrestrially sourced leaf waxes.

4. Results

4.1. Holocene chronology

The stratigraphy and geochemistry of tephra deposits on the Faroe Islands are well-characterized (Wastegård et al., 2018). Major oxide compositions from the Eiðisvatn glass shards are compared to previously identified tephra and cryptotephra horizons from the Faroe Islands and we attribute volcanic glass shards isolated from three discrete depth intervals in the Eiðisvatn record to the Hekla S, Hekla 4 and Saksunarvatn eruptions (Fig. 3; Tables 1 and 2). These three tephras, along with 13 radiocarbon dates, were used to build an age-depth model for the Eiðisvatn sediment core (Table 2, Fig. 4).

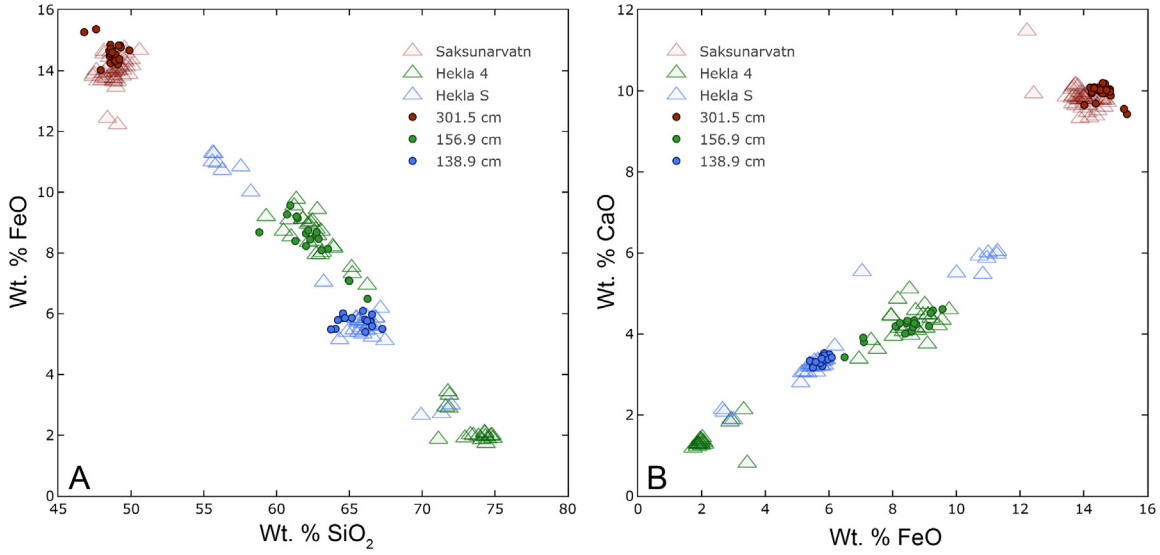

Fig. 3. Select major oxide compositions of three tephra layers from the Eiðisvatn record compared to previously described Icelandic tephra deposits on the Faroe Islands: (A) SiO_2 vs. FeO, (B) FeO vs. CaO. Glass shards from Eiðisvatn are compared to Hekla S (Wastegård et al., 2001, 2008, 2018), Hekla 4 (Hannon et al., 2001; Wastegård et al., 2001, 2018), and Saksunarvatn (Wastegård et al., 2001; Kylander et al., 2012).

Table 1
Geochemical composition of glass shards isolated from the Eiðisvatn record compared to tephra identified at other Faroe Islands sites.

Sample		SiO_2	TiO_2	Al_2O_3	FeO	MnO	MgO	CaO	Na_2O	K_2O	P_2O_5	Cl	BaO	Total
Eidi 138.9 cm (n = 15)	*Mean*	65.5	0.45	14.7	5.75	0.16	0.55	3.35	4.47	2	0.19	0.1	0.1	97.3
	1s	1.11	0.02	0.37	0.21	0.02	0.03	0.11	0.19	0.1	0.04	0	0	1.44
Hekla S (n = 15)[1,3]	*Mean*	66.6	0.4	14.7	5.28	0.16	0.48	3.21	4.45	2	0.11	–	–	97.3
	1s	2.32	0.11	0.46	1.09	0.04	0.16	0.8	0.55	0.4	0.04	–	–	1.49
Eidi 156.9 cm (n = 19)	*Mean*	62.7	0.63	14.1	8.25	0.26	0.5	4.14	4.38	1.8	0.18	0.1	0.1	97
	1s	1.93	0.13	0.46	0.99	0.03	0.21	0.35	0.57	0.2	0.07	0	0	1.6
Hekla 4 (n = 22)[1]	*Mean*	63.8	0.62	14.2	7.73	0.26	0.58	3.95	4.43	1.9	–	–	–	97.3
	1s	3.91	0.23	0.59	2.31	0.08	0.3	1.06	0.32	0.4	–	–	–	0.98
Eidi 301.5 cm (n = 24)	*Mean*	48.7	3.05	12.9	14.6	0.22	5.02	9.95	2.61	0.5	0.32	0	0	97.9
	1s	0.61	0.49	0.2	0.31	0.02	0.33	0.19	0.2	0.1	0.1	0	0	0.7
Saksunarvatn (n = 43)[1,2]	*Mean*	48.9	3.03	12.9	14	0.25	5.58	9.83	2.74	0.5	0.33	–	–	97.8
	1s	0.71	0.14	0.26	0.5	0.03	0.18	0.32	0.19	0	0.02	–	–	1.2

References: 1. Wastegård et al. (2001), 2. Kylander et al. (2012), 3. Wastegård et al. (2018).

Table 2
Chronological data used to construct Eiðisvatn age model.

Core	Composite Depth (cm)	Description	^{14}C age (yr BP)	Calibrated age range (cal yr BP, 1σ)	Median age (cal yr BP)
Surface	0				−65
EI-D-01-15	18.5	Plant macrofossil	−10	−5–−1	−3
EI-D-01-15	23	Plant macrofossil	410 ± 15	471–515	493
EI-P-01-15	25.86	Plant macrofossil	840 ± 30	710–784	747
EI-P-01-15	27.86	Plant macrofossil	3720 ± 70	3964–4176	4070[a]
EI-P-01-15	29.86	Plant macrofossil	2575 ± 20	2714–2760	2737[a]
EI-D-01-15	30	Plant macrofossil	1145 ± 15	986–1068	1027
EI-P-01-15	32.86	Plant macrofossil	2320 ± 20	2331–2355	2343[a]
EI-D-01-15	34	Plant macrofossil	1055 ± 35	924–1000	962
EI-D-01-15	35.86	Plant macrofossil	6355 ± 20	7257–7311	7284[a]
EI-P-01-15	39.5	Plant macrofossil	3030 ± 20	3179–3275	3227[a]
EI-D-01-15	40.2	Plant macrofossil	8110 ± 45	8985–9125	9055[a]
EI-P-01-15	43.86	Plant macrofossil	3915 ± 20	4316–4400	4358[a]
EI-D-01-15	57	Bulk organic matter	2450 ± 15	2471–2673	2572
EI-P-01-15	60.36	Bulk organic matter	2330 ± 20	2337–2355	2346
EI-D-01-15	82	Bulk organic matter	3300 ± 15	3492–3547	3520[a]
EI-P-01-15	96.16	Plant macrofossil	2945 ± 15	3076–3142	3109
EI-P-01-15	138.26	Plant macrofossil	3595 ± 15	3865–3925	3895
EI-P-01-15	138.86	Hekla-S Tephra		3700–3750	3720
EI-P-01-15	156.86	Hekla-4 Tephra		4240–4280	4260
EI-P-01-15	164.46	Plant macrofossil	4100 ± 30	4519–4703	4611
EI-P-01-15	174.96	Plant macrofossil	4310 ± 15	4844–4870	4857
EI-P-01-15	263.46	Bulk organic matter	7290 ± 30	8059–8145	8102
EI-P-01-15	278.46	Plant macrofossil	7925 ± 20	8645–8817	8731
EI-P-01-15	301.46	Saksunarvatn tephra		10136–10216	10176

[a] Indicates anomalously old radiocarbon ages that were not included in the final Eiðisvatn age model.

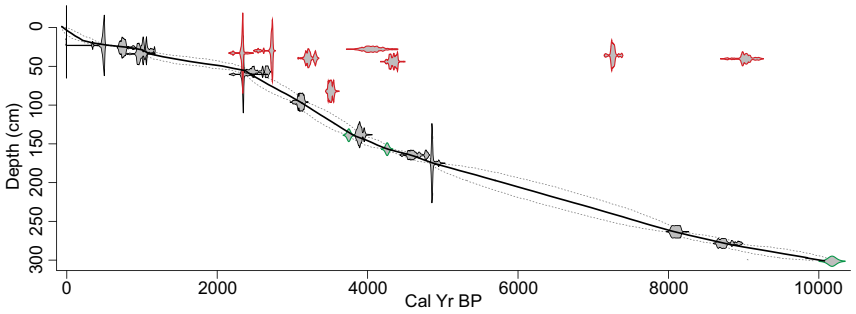

Fig. 4. Age model for Eiðisvatn sediment cores constructed using 'Bacon' in R (Blaauw and Christen, 2011). Grey shaded areas are probability distribution functions for individual dates. Red outlined symbols indicate radiocarbon outliers that were removed from the final age model. Black outlined symbols indicate radiocarbon ages that were used in the final age model. Green outlined symbols indicate tephra ages. Solid black line indicates median age model, and dashed line indicates 95% confidence interval. The average 95% confidence interval for sample ages is 454 years and the average amount of time represented by a 1 cm-thick sample is 33 years. (For interpretation of the references to color in this figure legend, the reader is referred to the Web version of this article.)

4.1.1. EI-P-01-15 138.9 cm/Hekla S (c. 3.7 ka BP)

The major oxide composition of dacitic to rhyolitic glass shards (n = 15) isolated from the interval 116.5–117.5 cm closely resembles the 3.7 ka Hekla Selsund (Hekla S) tephra horizon, which was previously identified in sediments from Faroese lakes Starvatn (Wastegård et al., 2008), Mjáuvötn (Wastegård et al., 2001), and

Havnardalsmyren (Wastegård et al., 2018). The composition of Hekla S deposits on the Faroe Islands varies between sites, likely due to geochemical differences between early and late eruption phases (Wastegård et al., 2018). Hekla S glass shards isolated from the Eiðisvatn record are geochemically similar to rhyolitic shards previously identified in sediments from Mjáuvötn and Havnardalsmyren (Wastegård et al., 2018, 2001), but distinct from andesitic shards found in sediments from Starvatn (Wastegård et al., 2008).

4.1.2. EI-P-01-15 156.9 cm/Hekla 4 (c. 4.3 ka BP)

We attribute dacitic to andesitic glass shards from the 135–136 cm depth interval (n = 19) to the Hekla 4 eruption c. 4.3 ka BP. As with Hekla S, the geochemical composition of Hekla 4 shards identified from the Faroe Islands is spatially heterogeneous. Tephra shards attributed to Hekla 4 from the Eiðisvatn core are geochemically similar to Hekla 4 glass shards previously found in bog sediments on the southwestern margin of Eiðisvatn, in lake sediments from Mjáuvötn(Wastegård et al., 2001) and a subset of shards from Havnardalsmyren (Wastegård et al., 2018, Table 1; Fig. 3). Their composition differs from rhyolitic shards found in sediments from Gróthusvatn (Hannon et al., 2001) and Havnardalsmyren that were attributed to Hekla 4 (Wastegård et al., 2018).

4.1.3. EI-P-01-15 301.5 cm/Saksunarvatn Ash (c. 10.2 ka BP)

The major oxide composition of most glass shards from the visible tephra horizon at the 140.5–141.5 cm (n = 24) depth interval closely resembles previously described deposits of the c. 10.2 ka BP basaltic Saksunarvatn Ash in the Faroe Islands (Wastegård et al., 2001; Kylander et al., 2012; Lohne et al., 2013, Table 1, Fig. 3). The Saksunarvatn Ash, with origins in the Grímsvotn volcanic system, is one of the most widely-dispersed Icelandic tephra deposits from the Holocene.

4.2. Holocene lithology and biomarker relative abundances

The Eiðisvatn sediment core is comprised primarily of dark brown gyttja. Fine laminations are visible in the bottom ~30 cm of the core, and the core terminates in a visible tephra layer. The sediment has an average LOI of ~15%, but ranges from 0% in the bottom tephra layer to 44%. The Eiðisvatn record was divided into four units based on the lithostratigraphy, biomarker abundances (Fig. 5), and isotope stratigraphy (Fig. 6).

Unit 1 (~10.0–8.1 ka) is the basal unit, which is comprised of finely laminated sediment with relatively low LOI (average of ~8.2%). This unit also has high relative abundances of C_{17} and C_{19} *n*-alkanes, which are typically attributed to algal and bacterial sources. The average *n*-alkane ACL is 29.3, and the average *n*-alkanoic

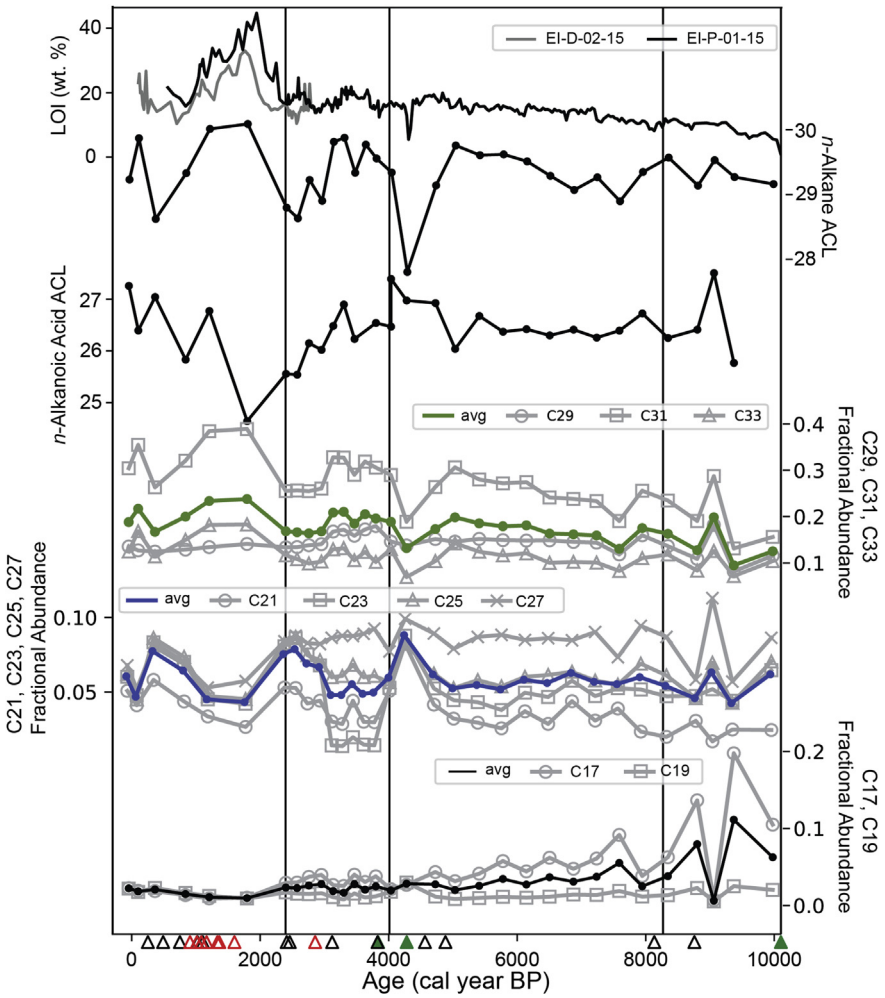

Fig. 5. Weight % Loss on Ignition measurements and plant wax distributions for the Holocene sediment core from Eiðisvatn. Triangles along x-axis indicate chronological tie points. Red triangles indicate radiocarbon age reversals that were excluded from age model, black triangles indicate radiocarbon ages that were included, and green triangles indicate tephra layers. (For interpretation of the references to color in this figure legend, the reader is referred to the Web version of this article.)

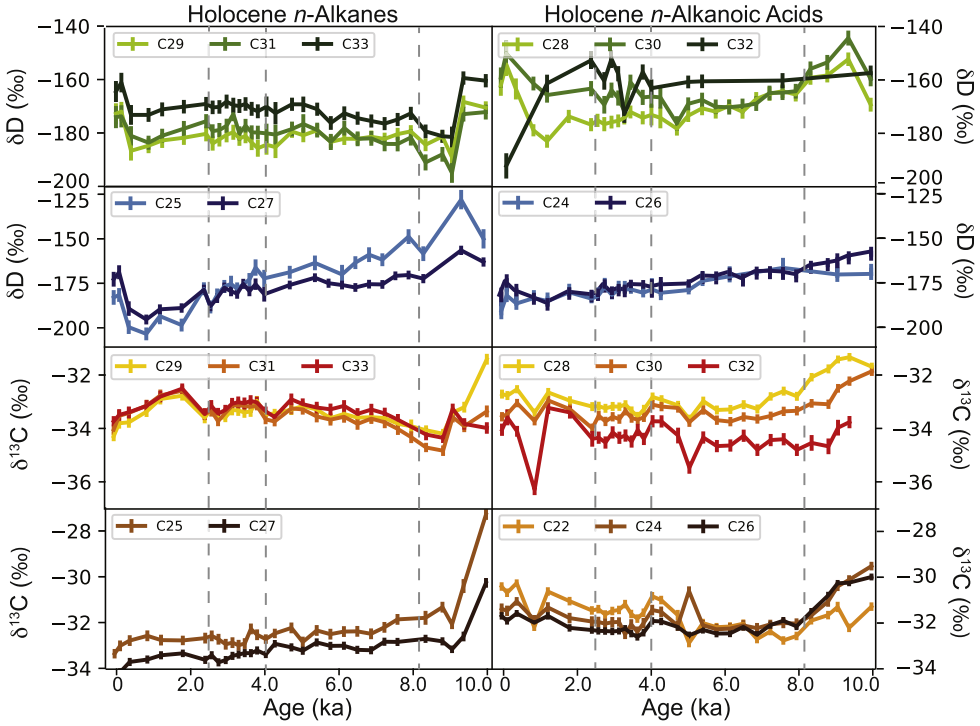

Fig. 6. Holocene *n*-alkane (left column) and *n*-alkanoic acid (right column) isotope values from the Eiðisvatn record. Green and blue panels show δD data for long- and mid-chain homologues, respectively. Red and brown panels show $\delta^{13}C$ data for long-chain and mid-chain homologues, respectively. Darkest color in each panel indicates longest chain length. Vertical dashed lines indicate Unit boundaries, as in Fig. 5 and 7. (For interpretation of the references to color in this figure legend, the reader is referred to the Web version of this article.)

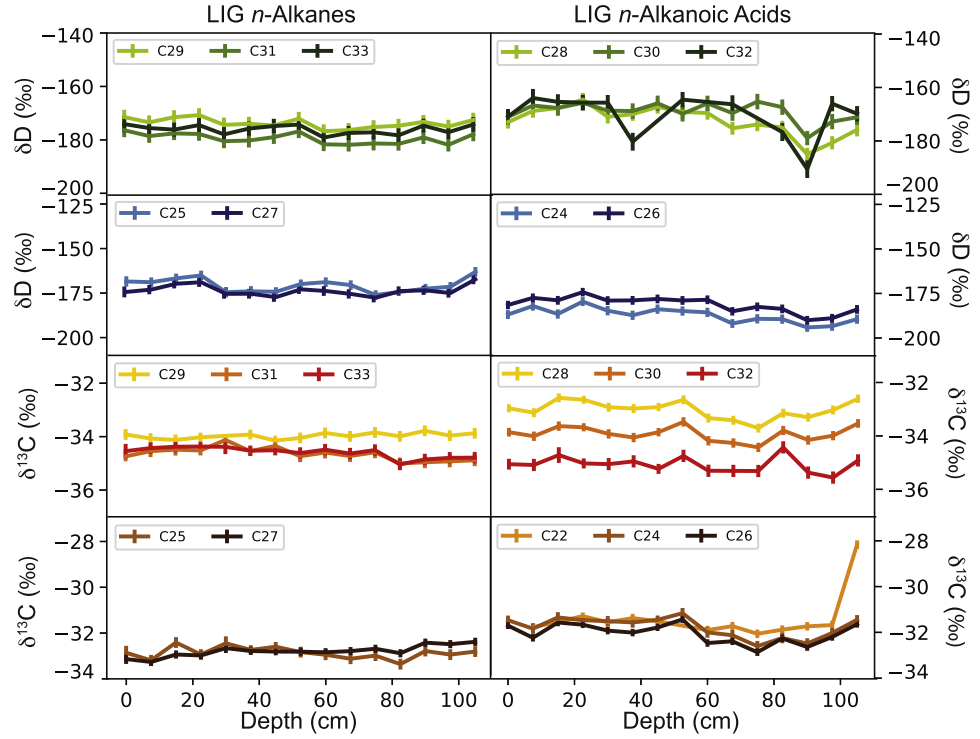

Fig. 7. LIG *n*-alkane (left column) and *n*-alkanoic acid (right column) isotope values from the Klaksvík section. Green and blue panels show δD data for long- and mid-chain homologues, respectively. Red and brown panels show $\delta^{13}C$ data for long-chain and mid-chain homologues, respectively. Darkest color in each panel indicates longest chain length. (For interpretation of the references to color in this figure legend, the reader is referred to the Web version of this article.)

acid ACL is 26.5.

Unit 2 (~8.1–4.0 ka) is comprised of dark brown gyttja, and has an average LOI of ~14%. The LOI increases steadily throughout Unit 2. The average *n*-alkane ACL is 29.4 and the average *n*-alkanoic acid ACL is 26.5. The sample from the Hekla-4 cryptotephra horizon has a low *n*-alkane ACL of 27.7 and also a low LOI value of 4.8%.

Unit 3 (4.0 – 2.4 ka) is also a dark brown gyttja, and has an average LOI of 17%. While the LOI increased steadily throughout Units 1 and 2, LOI is more variable in Unit 3, with two small, broad peaks that increase to ~20%. Both *n*-alkane and *n*-alkanoic acid ACLs decline across Unit 3, with average values of 29.1 and 26.3, respectively.

Unit 4 (2.4 – 0 ka) is the uppermost unit. This unit is a darker brown gyttja, and has an average LOI of ~27%. While the LOI increased almost linearly across Units 1–3, this unit has a large peak in LOI up to the maximum of 44%, which corresponds to the darkest interval in the core and also the anomalously old radiocarbon ages that were rejected from the age-depth model. Because this unit is characterized by an influx of apparently old carbon, it is possible that the radiocarbon ages that were not rejected from the model may also be older than the actual age of the sediment (Fig. 4). Thus, the age of the lower boundary of this unit is tentative, and further interpretation regarding the age of this transition should be made with caution. The *n*-alkane ACL increases to ~30 during the LOI peak while the *n*-alkanoic acid ACL decreases to 24.6. Average *n*-alkane ACL across Unit 4 is 29.4, and average *n*-alkanoic acid ACL is 26.2.

4.3. δD and $\delta^{13}C$ values of plant waxes

4.3.1. δD values of Holocene plant waxes

The plant waxes are grouped into in four different categories (Fig. 6): long-chain *n*-alkanes, including C_{29}, C_{31}, and C_{33}; mid-chain *n*-alkanes, including C_{25} and C_{27}; long-chain *n*-alkanoic acids, including C_{28}, C_{30}, and C_{32}; and mid-chain *n*-alkanoic acids, including C_{22}, C_{24}, and C_{26}.

The long-chain *n*-alkanes are most variable in Unit 1, where all homologues show a ~20‰ decrease in δD values between 9.3 ka and 9.0 ka and reach their minimum at 9.0 ka. After the initial drop, C_{31} and C_{33} δD values slowly increase upwards while C_{29} δD values remain stable.

In Unit 1, C_{33} has the most positive δD values, followed by C_{31} δD values, and C_{29} δD values are the most negative. In Unit 2 (~8.1–4.0 ka), C_{31} δD values and C_{33} δD values increase slightly while C_{29} δD values remain stable. After ~6.0 ka, C_{31} δD values become more positive than C_{29} δD values. δD values of all three homologues are stable throughout Unit 3. In Unit 4, their δD values decrease from 2.4 ka to 0.355 ka, after which they increase to the present.

Mid-chain *n*-alkane (C_{25} and C_{27}) δD values have a different trend during the Holocene compared to long-chain *n*-alkane δD values. Mid-chain *n*-alkane δD values are relatively high during Unit 1, and decrease gradually during Unit 2. In Unit 3, mid-chain *n*-alkane δD values decrease more rapidly. In Units 1–3, C_{25} δD values are more positive than C_{27} δD values, however in Unit 4 C_{27} becomes more positive. In Unit 4, mid-chain *n*-alkane δD values continue to decrease between 4.0 and 0.8 ka, after which they increase to their modern values. Overall, C_{25} values are highest in the earliest Holocene with a peak value of −128‰, and reach their minimum of −203‰ at ~0.8 ka. C_{27} δD values have a smaller range between −156‰ and −195‰.

In Units 1 and 2, C_{28} and C_{30} long-chain *n*-alkanoic acid δD values have a trend similar to the mid-chain *n*-alkanes. They have greatest values in Unit 1, and then slowly decrease throughout Unit 2. C_{28} δD values then remain stable throughout Unit 3, but the C_{30} *n*-alkanoic acid becomes more positive by ~10‰. In Unit 4, C_{28} δD values decrease from 2.0 to 1.2 ka, and then increase until present. C_{30} δD values remain stable from 2.0 to 1.2 ka, and then also increase until present. The C_{32} *n*-alkanoic acid was not abundant enough to measure δD on every sample but the δD values were more positive than the other homologues and generally follow the variability of C_{30} δD values in the later part of the record, then falling to the lowest Holocene value in the uppermost sample.

Mid-chain *n*-alkanoic acid δD values are less variable than any of the other homologues' δD values. In Unit 1, C_{26} δD values slowly decline while C_{24} δD values remain stable. Both C_{24} and C_{26} δD values decrease steadily across Units 2 and 3. In Unit 4, C_{24} continues to decrease, while C_{26} decreases from 2.4 to 1.2 ka, and then increases until present.

4.3.2. $\delta^{13}C$ values of Holocene plant waxes

Long-chain *n*-alkane $\delta^{13}C$ values mirror the long-chain δD values, with a sharp drop in Unit 1, slow rise through Unit 2, and relative stability during Unit 3. At the beginning of Unit 4 there is a 1‰ increase followed by decline to present. With the exception of the oldest sample (10.0 ka), C_{29}, C_{31}, and C_{33} $\delta^{13}C$ values are within analytical uncertainty of each other and follow the same trend.

The trends in the mid-chain *n*-alkane $\delta^{13}C$ values are less variable than mid-chain δD values, with the exception of the $\delta^{13}C$ value of the oldest sample which is ~2.5–3‰ more positive than the next oldest sample. Mid-chain *n*-alkane $\delta^{13}C$ values decline across Units 1 and continue to decline until ~7.0ka in Unit 2. C_{25} $\delta^{13}C$ values are stable through the rest of Units 2–4, until the decline from 355 cal yr BP to the present. C_{25} $\delta^{13}C$ values are more positive than C_{27} $\delta^{13}C$ values in each sample. C_{27} $\delta^{13}C$ values are more positive than long-chain *n*-alkane $\delta^{13}C$ values in Units 1 and 2, but are more negative in Units 3 and 4. C_{25} values are more positive than long-chain *n*-alkane $\delta^{13}C$ values in each sample.

Long-chain *n*-alkanoic acid $\delta^{13}C$ values have differing trends over the Holocene. C_{28} and C_{30} slowly decline in Unit 1 and Unit 2 until ~7.0 ka. They are stable for the remainder of the record, through Units 2–4. The trends in C_{32} $\delta^{13}C$ values, however, are more similar to long-chain *n*-alkane $\delta^{13}C$ values. They decline abruptly in Unit 1, increase across Unit 2, and are relatively stable during Unit 3. The C_{32} $\delta^{13}C$ values then increase across the transition into Unit 4 and decline until present (with one outlier).

Of the mid-chain *n*-alkanoic acids, C_{26} and C_{24} $\delta^{13}C$ values decline across Unit 1 and remain stable across Units 2 and 3. They increase throughout Unit 4 to present. C_{22} $\delta^{13}C$ values are ~1.5‰ more negative than C_{26} and C_{24} at the beginning of Unit 1 and are relatively stable across this interval. C_{22} $\delta^{13}C$ values are stable across Unit 2 until an abrupt increase ~5.0 ka, and then remain stable for the remainder of Unit 3. C_{22} $\delta^{13}C$ values then increase across Unit 4.

4.3.3. δD and $\delta^{13}C$ values of LIG plant waxes

LIG long-chain *n*-alkane δD values (Fig. 7) show little variability over the length of the record. C_{29} δD values are the most positive, followed by C_{33}, and C_{31} δD values, which are the most negative. Long-chain *n*-alkane δD values have averages of −174‰, −179‰, and −176‰ for C_{29}, C_{31}, and C_{33}, respectively. Mid-chain *n*-alkane δD values also show little variability. C_{25} δD values are slightly more positive in some samples, but C_{27} and C_{25} δD values are within analytical uncertainty of one other for most samples. The average C_{25} δD value for this record is −170‰, and the average C_{27} value is −173‰.

LIG long-chain *n*-alkanoic acid δD values (Fig. 7) also show little variability, with the exception of one sample (depth = 82.5 cm) in which all three homologues are more negative. C_{30} δD values are more positive than C_{28} δD values, and they have average values of −169‰ and −172‰, respectively. The LIG mid-chain *n*-alkanoic

acids also have low variability in δD values. The δD values of C_{24} are slightly more positive than those of C_{26}, with an average δD value of −187‰, and C_{26} has an average δD value of −181‰.

LIG wax $\delta^{13}C$ values (both *n*-alkanes and *n*-alkanoic acids) are also relatively constant within the section. C_{33} and C_{31} *n*-alkane $\delta^{13}C$ values are the same (within error), while C_{29} $\delta^{13}C$ values are slightly more positive. C_{33} and C_{31} $\delta^{13}C$ values both average −34.6‰, and C_{29} has an average value of −34.0‰. The mid-chain *n*-alkane $\delta^{13}C$ values are very similar to each other, and are both more positive than the long-chain *n*-alkane $\delta^{13}C$ values. C_{27} has an average value of −32.8‰ and C_{25} has an average value of −32.9‰.

Long-chain *n*-alkanoic acid $\delta^{13}C$ values are consistently offset from one another by ~1‰. The average $\delta^{13}C$ values for C_{28}, C_{30}, and C_{32} are −33.0‰, −33.9‰, and −35.1‰, respectively. The mid-chain *n*-alkanoic acid $\delta^{13}C$ values are very similar to one another, with the exception of one outlier. The mid chain*n*-alkanoic acids $\delta^{13}C$ values are also more positive than the long-chain values, with average values of −31.7‰, −31.8‰, and −32.1‰ for C_{22}, C_{24}, and C_{26}, respectively.

5. Discussion

5.1. Plant wax sources

Understanding the sources of plant waxes is important for interpreting the climate signals contained in the δD records. Plant wax molecules are usually attributed to different types of vegetation according to the length of their carbon chains; short-chain lipids (17–20 carbon atoms) are produced by aquatic algae and bacteria, mid-chain lipids (21–26 carbon atoms) are produced by submerged aquatic plants, and long-chain lipids (27–35 carbon atoms) are produced in the leaf waxes of terrestrial plants (Cranwell et al., 1987; Eglinton and Hamilton, 1967; Ficken et al., 2000). While individual plant species may produce a variety of chain lengths (Diefendorf et al., 2011), when integrated through space and time in a sedimentary record, the isotopes of hydrogen and carbon in the biomarkers can be attributed to more specific sources than isotopes of organic material in bulk sediment (Sachse et al., 2012). If different individual or groups of waxes can be attributed to primarily aquatic or terrestrial sources, then past changes in precipitation isotopes and local hydroclimate can be inferred (Rach et al., 2017; Sachse et al., 2012; Seki et al., 2011).

The trends in the δD values of *n*-alkanes and *n*-alkanoic acids in the Eiðisvatn record can be grouped by wax type and the chain length (Fig. 8). We would expect that waxes derived from the same sources have similar trends in δD values, even if the values are offset. Notably, the long-chain and mid-chain *n*-alkane δD values show very different trends, and the δD records of all chain lengths of *n*-alkanoic acids are more similar to the mid-chain *n*-alkane δD records in units 1–3 (Fig. 8). From this, we infer that the long-chain *n*-alkanes record a signal from one source (terrestrial plants), while the mid-chain *n*-alkanes and the *n*-alkanoic acids record a signal from another source (aquatic macrophytes).

While all wax groups likely receive contributions from both terrestrial and aquatic sources, the carbon isotope ratio ($\delta^{13}C$) of plant waxes can provide insight concerning the dominant sources of individual plant wax homologues. The $\delta^{13}C$ of plant waxes reflect the isotopic composition of their CO_2 source, in addition to the fractionation that occurs during biosynthesis. Terrestrial plants source CO_2 from the atmosphere, while aquatic plants source CO_2 from lake water dissolved inorganic carbon (DIC). DIC is generally enriched in ^{13}C due to the uptake of ^{12}C by photosynthetic organisms in surface waters (Meyers and Teranes, 2001). This can cause aquatic plants to be enriched in ^{13}C compared to terrestrial plants,

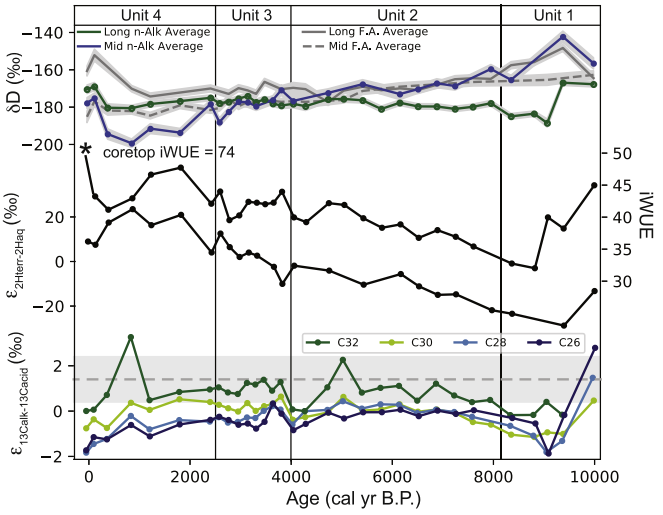

Fig. 8. Top: Average *n*-alkane and *n*-alkanoic acid δD values in the Holocene (green: long-chain *n*-alkane δD values, blue: mid-chain *n*-alkane δD values, solid grey: long-chain *n*-alkanoic acid δD values, dashed grey: mid-chain *n*-alkanoic acid δD values). Middle: Hydroclimate proxies in the Holocene record, including calculated iWUE and $\varepsilon_{terr\text{-}aq}$. Bottom: Calculated offset between biosynthetically equivalent *n*-alkanes and *n*-alkanoic acids ($\varepsilon_{n\text{-}alk\text{-}acid}$) for each sample in the Holocene record. Grey dashed line and shaded region indicates published average value ± 1σ error. (For interpretation of the references to color in this figure legend, the reader is referred to the Web version of this article.)

which has been observed in the Faroe Islands and in similar environments in Iceland (Langdon et al., 2010; Olsen et al., 2010). The carbon isotopic enrichment of aquatically sourced waxes is evident within the wax groups, in that shorter carbon chains have more positive $\delta^{13}C$ values than longer chains in almost every sample from both Eiðisvatn (Fig. 6) and the Klaksvík section (Fig. 7), and previous studies report that there is no systematic difference in $\delta^{13}C$ values of homologous waxes from individual plants (Chikaraishi and Naraoka, 2007, 2003). Therefore, while each homologue within a sediment sample likely represents a mixture of sources, we can use $\delta^{13}C$ values as an indicator of whether aquatic or terrestrial components are the dominant source for each homologue.

The *n*-alkanoic acids from Eiðisvatn and Klaksvík sediment are more enriched in ^{13}C than would be expected given the $\delta^{13}C$ value of the biosynthetically equivalent *n*-alkane, which suggests that they are predominantly produced by an aquatic macrophyte source. Modern plant studies of $\delta^{13}C$ across wax types show that *n*-alkanes are enriched compared to their *n*-alkanoic acid biosynthetic equivalents (Chikaraishi and Naraoka, 2007) by up to 7‰ in $\delta^{13}C$. The apparent fractionation of ^{13}C between *n*-alkanes and *n*-alkanoic acids ($\varepsilon_{13Calk\text{-}13Cacid}$) averages 1.4 ± 1.1‰ regardless of plant type or photosynthetic pathway (Chikaraishi and Naraoka, 2007). We would thus expect the sedimentary waxes to have similar $\varepsilon_{13Calk\text{-}13Cacid}$ values if they are derived from the same source. $\varepsilon_{13Calk\text{-}13Cacid}$ values calculated for the C_{30} *n*-alkanoic acid/C_{29} *n*-alkane, the C_{28} *n*-alkanoic acid/C_{27} *n*-alkane, and the C_{26} *n*-alkanoic acid/C_{25} *n*-alkane from Holocene samples in the Faroe Islands are less than 1.4‰ in most samples, and in many cases $\varepsilon_{13Calk\text{-}13Cacid}$ is negative (Fig. 8). This implies that the *n*-alkanoic acid $\delta^{13}C$ values are more positive than they would be if they had the same source as the *n*-alkanes, which supports our interpretation that the *n*-alkanoic acids are primarily aquatically sourced.

While long-chain *n*-alkanoic acids are commonly attributed to terrestrial sources, in some settings *n*-alkanoic acids as long as C_{28} have been found to be aquatically-derived or from mixed sources (Holland et al., 2013; van Bree et al., 2018). In the Eiðisvatn

sediments, $\varepsilon_{13Calk\text{-}13Cacid}$ values for the C_{32} *n*-alkanoic acid are the most positive, suggesting that C_{32} *n*-alkanoic acids have more of a terrestrial signature than the other *n*-alkanoic acids. However, in these samples the C_{32} *n*-alkanoic acid has very low abundances, making it difficult to measure its δD values. The trend in the δD values of the C_{30} *n*-alkanoic acid are consistent with the mid-chain *n*-alkane δD records only from 10.0 ka to ~6.0 ka, and during this period $\varepsilon_{13Calk\text{-}13Cacid}$ is very low, which is consistent with a predominantly aquatic source. In the latter half of the Holocene, the δD values of the C_{30} *n*-alkanoic acid no longer follow the trend of the mid-chain *n*-alkane δD record, however they do not exactly follow the long-chain *n*-alkane δD trend either. The C_{30} *n*-alkanoic acid is likely derived from a mixture of terrestrial and aquatic sources, reflected in the higher $\varepsilon_{13Calk\text{-}13Cacid}$ values from ~6.0ka to present.

Trends in the Holocene $\varepsilon_{13Calk\text{-}13Cacid}$ values reveal changes in the relative proportion of terrestrial and aquatic contributions to the plant waxes that are preserved. The $\varepsilon_{13Calk\text{-}13Cacid}$ values for all the plant wax pairs are most negative during Unit 1, indicating that the proportion of aquatically derived *n*-alkanoic acids was greatest at this time, or that the *n*-alkanoic acids that are produced have more positive $\delta^{13}C$ values. This suggests that there was a higher proportion of autochthonous material being deposited in Eiðisvatn in the early Holocene, which can either be accomplished by a reduction in terrestrial input or enhanced aquatic productivity. Unit 1 also has the highest relative abundances of C_{17} and C_{19} *n*-alkanes, the production of which is attributed to algae (Cranwell et al., 1987), which is also consistent with a higher proportion of autochthonous organic matter being deposited. Pollen records suggest that following deglaciation around 11.2 ka, the early Holocene in the Faroes was characterized by fell-field vegetation and poor soil development (Hannon et al., 2010, 2003; Johansen, 1985). If the terrestrial biomass was small and soils were thin, there would be less terrestrially sourced material delivered to the lake. $\varepsilon_{13Calk\text{-}13Cacid}$ values for all wax pairs are stable throughout Units 2 and 3, and decline again in Unit 4. This suggests that the proportion of aquatic vs terrestrial *n*-alkanoic acids is relatively constant through the mid-Holocene, and the latest Holocene is characterized by a slightly increased aquatic contribution.

5.2. Holocene climate

5.2.1. Precipitation isotopes

In the Faroe Islands, the δD of lake water represents the isotopic composition of precipitation, and therefore we interpret mid-chain *n*-alkane and *n*-alkanoic acid δD values as recorders of past precipitation isotopes. In a wet, cool environment, like the Faroes, evaporative enrichment of lake water is minimal. Lake water collected from Faroese lakes that are currently hydrologically open have δD and $\delta^{18}O$ compositions that fall on the local meteoric water line for the Reykjavik GNIP station (Fig. 2), indicating that little evaporation has occurred. The average δD values of these lake water samples (−36.5‰) are very similar to the OIPC modeled precipitation for August (−39‰), the month that the samples were collected. Because the mid-chain *n*-alkanes and most of the *n*-alkanoic acids (C_{30} and shorter) are primarily aquatically derived, we expect that they are recording past changes in lake water isotopes during the growing season, from which we can infer past changes in spring-summer precipitation isotopes.

Precipitation δD values at mid-latitudes are strongly influenced by regional temperatures, changes in moisture source and/or local changes in hydroclimate. The location, temperature, and relative humidity of the oceanic moisture source influence the initial isotopes of precipitation in a given air mass; the trajectory of the air mass, amount of rainfall along that trajectory, and additional moisture added to the air mass through evaporation of surface waters influence the intermediate isotopic composition; the seasonality of precipitation and the local temperature and relative humidity during condensation affect the final isotopes of precipitation (Boyle, 1997; Dansgaard, 1964; Pierrehumbert, 1999). In the North Atlantic today, heat and moisture carried northward by ocean and atmospheric transport cause the region (including the Faroe Islands) to have anomalously positive isotopes in precipitation for its latitude (Bowen and Revenaugh, 2003).

Given the numerous controls on precipitation isotopes in the region, rather than interpreting precipitation isotopes strictly as a quantitative indicator of temperature, we use the δD data to infer regional climatology. During periods with enhanced northward oceanic heat transport by the North Atlantic Current, for instance due to more vigorous meridional overturning circulation, greater heat and moisture are transported to the North Atlantic resulting in more positive precipitation isotopes values in the North Atlantic region. During periods with reduced northward oceanic heat transport, for instance due to weaker overturning circulation, regional temperatures cool, less Atlantic-sourced precipitation reaches the Faroe Islands and the moisture that does is subject to greater rainout and isotopic fractionation prior to arrival, and the isotopes in precipitation become more negative.

In our Eiðisvatn record, δD values of mid-chain *n*-alkanes and *n*-alkanoic acids indicate an overall decrease in the isotope values of precipitation during the course of the Holocene (Fig. 8). We interpret this trend to reflect a decrease in the northward transport of heat and moisture in the North Atlantic region. This trend generally matches the declining trend in Northern Hemisphere summer insolation and the documented decline in regional summer temperatures over the same period (Marcott et al., 2013). The most positive isotope values in the Eiðisvatn record occur during Unit 1, suggesting an early regional thermal maximum. A major decline begins within Unit 3, likely signaling cooling temperatures and less Atlantic-sourced precipitation during the Neoglacial period. These trends broadly match local qualitative temperature records from the Faroe Islands, which indicate a thermal maximum ~9.0 to 8.0 ka, cooling from ~8.0 ka to 4.0 ka, and intensified cooling until present (Hannon et al., 2010; Johansen, 1985, 1981; Olsen et al., 2010). This is also consistent with the closest Holocene sea surface temperature reconstruction, which shows peak Holocene temperatures from 10.3 ka to 8.3 ka and declining temperatures until modern (Rasmussen and Thomsen, 2010). Regional SSTs also generally match this trend (Ayache et al., 2018; Marcott et al., 2013; Marsicek et al., 2018). The reason for increased northward ocean heat transport in the early to mid-Holocene is likely linked to enhanced overturning circulation and deep water convection processes in the Nordic seas at this time (Thornalley et al., 2013).

We note that the decrease in precipitation δD values throughout the Holocene in the Faroe Islands could also be interpreted as a shift toward a greater amount of wintertime precipitation. However, we reject this interpretation on a number of grounds. Firstly, δD values of plant waxes are likely to be biased toward precipitation isotope values during the growing season, i.e. spring and summer. The isotopic values of modern lake water samples are most similar to precipitation in the month that they were collected (August) rather than the mean annual precipitation value predicted by OIPC. This suggests that the δD values of aquatically derived plant waxes are likely recording lake water/precipitation water δD values in late spring and summer and would not reflect seasonal changes in precipitation isotopes. Secondly, the seasonal range in the isotopes of precipitation of the Faroe Islands, as calculated by the OIPC (Bowen, 2019), is relatively small (~50‰; Fig. 2). Even under the most extreme case, assuming 100% of annual precipitation in the Early Holocene fell during the summer season, precipitation isotope values would not increase by the magnitude inferred from

the plant wax δD values; instead, the data indicate that early Holocene precipitation isotopes were more positive than in the late Holocene. Additionally, because OIPC-predicted summer precipitation isotope values may be overestimated, it is even less likely that seasonal shifts alone can account for the inferred 35‰ decrease in precipitation isotope values over the Holocene.

5.3. Holocene hydroclimate

The difference between a terrestrial plant-derived wax δD record (δD_{terr}) and an aquatic-plant-derived wax δD record (δD_{aq}) represents watershed-integrated soil water evaporative enrichment and plant evapotranspiration, which are generally attributed to changes in relative humidity (Nichols et al., 2010; Rach et al., 2017; Seki et al., 2011). As stated in Section 5.2, Faroese lake water isotopes are expected to reflect changes in precipitation isotopes because the lake water experiences little evaporative enrichment, and thus mid-chain plant wax δD values track precipitation isotopes. But, soil and therefore leaf waters can experience evaporative enrichment, depending on local relative humidity (Sachse et al., 2004; Ziegler, 1989). A comparison of plant water and lake water isotope reconstructions based on long-chain and mid-chain wax δD values, respectively, can reflect evaporative enrichment of precipitation water, which can be attributed to changes in local hydroclimate (Nichols et al., 2010; Rach et al., 2017; Seki et al., 2011). We interpret the fractionation between δD_{terr} and δD_{aq} ($\varepsilon_{2Hterr\text{-}2Haq}$) to represent the amount of evaporative enrichment of soil and leaf water. We find an increasing trend in $\varepsilon_{2Haq\text{-}2Hterr}$ after 9.0 ka, indicating a drying trend over most of the Holocene (Fig. 8).

Carbon isotope values of terrestrial plant waxes can also reflect local hydrology. In terrestrial plants, the fractionation of carbon isotopes during photosynthesis is controlled by the fractionation associated with gas diffusion through the stomata and the fractionation of the Rubisco enzyme (Farquhar et al., 1982). When the environment becomes drier, the stomata on a plant's leaves close to reduce evaporative loss of water, which reduces the fractionation between atmospheric CO_2 and plant wax carbon, increasing plant wax $\delta^{13}C$ values. Therefore, terrestrial plant carbon isotopes can also be used to infer past changes in moisture due to changes in leaf-level isotopic fractionation ($\varepsilon_{13Catm\text{-}13Cplant}$) that are associated with changing stomatal conductance and intrinsic water use efficiency (iWUE) (Ehleringer et al., 1993). iWUE increases over the Holocene, which is consistent with the drying trend interpreted from $\varepsilon_{2Haq\text{-}2Hterr}$.

Changes in carbon assimilation that are unrelated to moisture availability can also impact the water use efficiency of plants and can complicate $\delta^{13}C$-based hydroclimate interpretations. If other environmental factors such as increased light exposure or increased nutrients increase the photosynthetic capacity of a plant, c_i is reduced and the carbon isotopic values of plant material become enriched, which is also expected at higher iWUE. Mesophyll conductance, or the diffusion of CO_2 between substomatal cavities to the cite of CO_2 fixation, is also an important factor for iWUE that is independent of hydrologically-driven changes in stomatal conductance (Seibt et al., 2008). By evaluating δD and $\delta^{13}C$ together, those effects can be disentangled; if δD and $\delta^{13}C$ co-vary it is likely that changes in relative humidity are the drivers (Scheidegger et al., 2000), while a negative correlation suggests a change in photosynthetic capacity as the main driver of $\delta^{13}C$ changes. iWUE shows similar trends to $\varepsilon_{2Haq\text{-}2Hterr}$ (Fig. 8), with higher iWUE when there is more inferred evaporative enrichment of water isotopes. Thus, we infer from both proxies that a reduction in relative humidity occurred throughout the course of the Holocene.

Shifts in vegetation type in the watershed can also affect plant wax δD and $\delta^{13}C$ values, independent of hydroclimatic change. The shift in long-chain plant wax δD and $\delta^{13}C$ around 9.3 ka is likely due to a change in vegetation. The period between 10.5 ka and 9.0 ka was characterized by a rapid rise and decline of *Betula nana* and a rapidly changing climate in the Faroe Islands (Hannon et al., 2010, 2003; Jessen et al., 2008; Johansen, 1985, 1981, 1975), after which the climate became more mild and vegetation became dominated by sedges, heath, and juniper scrub. After 9.0 ka and before 2.4 ka, there is no indication of major, sudden shifts in vegetation based on plant wax distributions (Fig. 5) or from published pollen records that span the Holocene (Johansen, 1985, 1975).

Hydroclimate reconstructions from the Arctic and North Atlantic regions are scarce compared to temperature reconstructions (Sundqvist et al., 2014), however they are critical to understanding past changes in the climate system. Reconstructions of glacier size in western Norway, which are thought to be dominantly controlled by winter precipitation amount, suggest that some regions experienced wetter conditions in the neoglacial period (Bakke et al., 2008) while others experienced drier conditions (Bjune et al., 2005). Pollen and lake level records from Northern Scandinavia also diverge, with some indicating a drying trend over the Holocene (Bigler et al., 2002; Hammarlund et al., 2003) and some showing little hydrological changes after 6.0 ka (Seppa and Birks, 2001). Southern Scandinavian lake levels appear to have increased after 4.0 ka (Hammarlund et al., 2003), and a reduction in the humification of peat in northern Scotland after 3.9 ka indicate wetter neoglacial conditions (Anderson et al., 1998). Our results from the Faroe Islands suggest a shift to drier conditions in the late Holocene.

5.4. The last 2.4 ka

The Eiðisvatn core provides evidence for a major environmental shift beginning at ~2.4 ka (Unit 4). This is perhaps most obvious in the LOI signal, which increases to ~40% during this time. At the same time as the LOI peak, there are eight anomalously old radiocarbon ages. This implies a sudden input of old organic material, indicating rapid erosion that is documented elsewhere in the Faroes during the late Holocene (Hannon et al., 2005; Lawson et al., 2005; Olsen et al., 2010). Associated with the peak in LOI, there is an increase in the $\delta^{13}C$ values of long-chain *n*-alkanes (Fig. 6), potentially due to changes in vegetation associated with peat and/or grassland formation in the watershed. Additionally, there is a notable change in the distribution of plant waxes after 2.4 ka, primarily a large increase in the amount of C_{31} and C_{33} *n*-alkanes leading to higher *n*-alkane ACL (Fig. 5). C_{31} and C_{33} are often attributed to grasses (Maffei, 1996), and this probably reflects a transition to grassland from a heath, sedge, and shrub-dominated landscape.

The environmental shift that is recorded at 2.4 ka in the Eiðisvatn record could be related to early human settlement on the Faroe Islands. Evidence from pollen records confirm that large, wild grass types (which, on Iceland, are an indication of human settlement) were present before 2.82 ka (Hannon and Bradshaw, 2000). The first microcharcoal evidence of human settlement was dated to 1.38 ka (Hannon et al., 2005). A paleobotanical settlement horizon at Eiðisvatn was dated to between 1.3 and 1.55 ka (Hannon et al., 2001). Our evidence of landscape change predates the pollen evidence significantly; however, uncertainties in the age model after 2.4 ka make it difficult to conclude whether this disturbance interval is coincident with the paleobotanical changes observed by Hannon et al. (2001) and others, or if it indicates that erosion began to occur before the appearance of cereals and charcoal. Because of a lack of tall, deep-rooting plants, it is possible that the landscape was particularly sensitive to minor changes in climate, and late-

Holocene cooling triggered erosion in the watershed. Without compelling evidence of human settlement in the Faroes during this disturbance interval, its cause remains enigmatic.

5.5. Interglacial climate comparison

Mid-chain alkane δD values from the late LIG Klaksvík sediment, which are interpreted to represent precipitation δD, are similar to Holocene δD values from 8.1 to 4.0 ka (Fig. 9), and are approximately 20‰ more positive than the average for the last 2.4 ka. This implies that late LIG regional temperatures were higher than the late Holocene, but similar to those of the early and middle Holocene. Furthermore, the late LIG $\varepsilon_{2Hterr\text{-}2Haq}$ values are most similar to Holocene values from Unit 2, and late LIG iWUE values are most similar to Holocene values from Unit 1 (Fig. 9), suggesting that the late LIG was wetter than the mid-late Holocene. Previous studies of the Klaksvík LIG section have found *Ajuga,* statoblasts of *Cristatella mucedo*, and *Betula* sect. *Albae*, which suggest that summer temperatures were slightly higher than modern conditions (Bennike et al., 2018; Wastegård et al., 2005). Other than those few differences, most of the pollen and macrofossils from the late LIG section in the Faroes indicate that the vegetation was similar to the pre-settlement vegetation of the Holocene (Bennike et al., 2018; Wastegård et al., 2005).

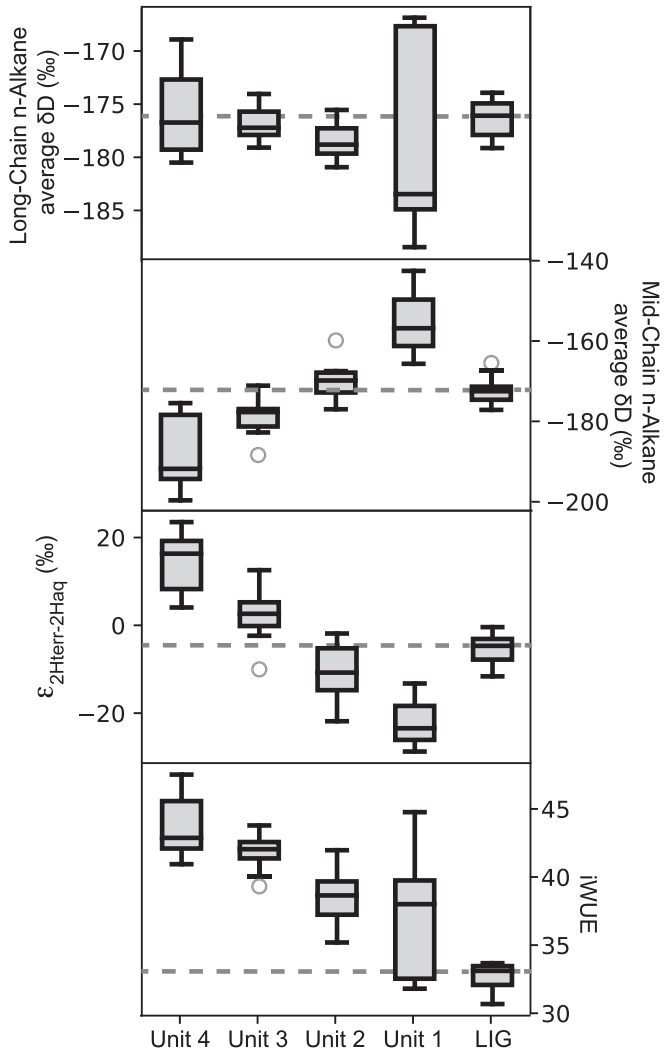

Fig. 9. Comparison of LIG and Holocene plant wax δD values and paleohydrological proxies in the Faroe Islands. Box and whisker plots for each unit of the Holocene record for comparison to all LIG values. Dashed grey line indicates mean of the LIG values.

Global temperatures during the LIG are generally thought to have been higher than the present interglacial due to higher summer insolation, evidenced by higher temperatures in the Greenland (NEEM Community Members, 2013) and Antarctic (Jouzel et al., 2007) ice core records, sea level that was 6–9 m higher than present (Dutton et al., 2015), various marine and terrestrial proxy records (Capron et al., 2014; Kaspar et al., 2005; Turney and Jones, 2010), and climate model simulations (Gierz et al., 2017; Otto-Bliesner et al., 2013). As discussed in section 5.2.1, the δD of precipitation in this location represents temperature, moisture sources, and regional temperature gradients related to the amount of ocean and atmospheric heat transport from lower latitudes. Modeling studies of precipitation isotopes during the LIG indicate that annually averaged precipitation isotopes may have been more negative in the North Atlantic during the LIG compared to modern (Gierz et al., 2017). Summer precipitation shows slightly more positive isotope values in the North Atlantic for the 125 ka time slice, but more negative values for 120 and 130 ka (Gierz et al., 2017). This suggests that even if global temperatures were warmer and precipitation isotopes in other regions were more positive, the North Atlantic and more specifically the Faroe Islands may be an exception, and overall the climate in this part of the North Atlantic may have been very similar to the Holocene during the LIG.

Because of the uncertainty inherent in dating terrestrial LIG archives, it is difficult to ascertain precisely which part of the LIG the Klaksvík section captures, however previous studies have suggested that it encompasses the late LIG and does not include the beginning of the LIG period. Greve (2001) inferred that the Klaksvík sequence spans approximately 5ky-8ky after 124 ka through a comparison of the Klaksvík pollen sequence to European pollen sequences from the Eemian (Zagwijn, 1996) and the presence of the 53-Midt/RHY tephra. Given the Holocene sedimentation rate we observe in our Eiðisvatn record, it is reasonable that the ~1 m of LIG sediment could represent 5–8 ky of the late LIG. The chronological uncertainties for the LIG section at Klaksvík are not unique to this location, due to the difficulties in dating terrestrial material from the LIG. However, the section at Klaksvík still provides a useful snapshot of late LIG conditions at this North Atlantic site.

Paleoclimate records and modeling studies show different peak warming periods during the LIG (Capron et al., 2014; Otto-Bliesner et al., 2013; Pfeiffer and Lohmann, 2016). Some marine records in the North Atlantic and the NEEM ice core show early peak warming (~130ka), followed by cooling, generally matching the LIG northern hemisphere summer insolation curve (Cortijo et al., 1994; Fronval et al., 1998; Manthé, 1998; Oppo et al., 2006). However, the two closest marine sea surface temperature records (MD95-2009 and ENAM 33) on either side of the Iceland-Faroe Ridge show late peak warmth, after the deposition of the 53-Midt/RHY tephra that is present in both the Klaksvík section and the MD95-2009 record (Capron et al., 2014; Manthé, 1998; Rasmussen et al., 2003). While it is possible that peak warmth occurred early in the LIG, and that the late LIG sequence preserved in the Faroe Islands does not encompass the warmest interval of the LIG period, these local sea surface temperature records suggest delayed warming in the North Atlantic region relative to insolation forcing, unlike Holocene SST records and our record from the Faroes, which suggests that regional temperatures and northward moisture transport were closely tied to insolation forcing and peaked during the early Holocene. Van Nieuwenhove et al. (2011) attribute the delayed incursion of warm North Atlantic waters in the Nordic Seas to lingering effects of the Saalian Ice Sheet and the boundary conditions created by different ice sheet configurations following Termination II.

Although our data cannot speak to conditions during the early LIG, they do indicate warmer-than-present conditions during the late LIG period and are consistent with local SST records that suggest late LIG warming.

Despite the age uncertainties of the Klaksvík sediment, comparison of the same climate proxy in nearly the same geographic locations allows us to place this snapshot of the late LIG in the context of the climate evolution of the Holocene. It is well-established that most of the North Atlantic and Arctic was warmest during the early-to mid-Holocene, and that preindustrial and Little Ice Age temperatures are potentially the coldest since the last glacial period or the Younger Dryas (Marcott et al., 2013; Marsicek et al., 2018). Here, we infer that late LIG conditions in this region were similar to early Holocene conditions.

6. Conclusion

We report Holocene and late Last Interglacial (LIG) paleoclimate reconstructions from Lake Eiðisvatn on the island of Eysturoy and a lacustrine sediment unit from Klaksvík, Borðoy Island in the Faroe Islands, based on hydrogen and carbon isotopes of sedimentary plant waxes. The trends in hydrogen isotope values of terrestrially- and aquatically-derived plant waxes are used to infer that the Faroe Islands became progressively drier and that there was a reduction in the northward transport of heat by the ocean and atmosphere to the northern North Atlantic throughout the course of the Holocene. This conclusion is based on the interpretation that the hydrogen isotopes of long-chain *n*-alkanes reflect the isotopic composition of soil and leaf water that was subject to isotopic enrichment due to evaporation, while the shorter chain *n*-alkanes reflect lake water that tracks precipitation isotopes. The carbon isotopes of long-chain *n*-alkanes, which reflect the intrinsic water use efficiency of terrestrial plants, support this interpretation and suggest that moisture availability decreased throughout the Holocene. This study provides the first Holocene paleohydrologic reconstruction for the Faroe Islands. By comparing the same climate proxy measurements to those made on plant waxes preserved in late LIG-aged sediments, we are able to place the climate conditions of the late LIG in the Faroe Islands into the context of Holocene climate and to conclude that late LIG climate in the Faroe Islands was warmer and wetter than present, and most similar to the conditions of the mid to early Holocene.

Acknowledgements

This research was supported by NSF grant NSF-BCS-16-23595 to WJD, NB, and RB. We would like to thank Jostein Bakke for assistance in the field, and Nicole DeRoberts for assistance in the LDEO Organic Geochemistry Laboratory. We also acknowledge two anonymous reviewers, whose comments helped to improve this manuscript.

References

Anderson, D.E., Binney, H.A., Smith, M.A., 1998. Evidence for abrupt climatic change in northern Scotland between 3900 and 3500 calendar years BP. Holocene 8, 97–103.

Andresen, C.S., Björck, S., Rundgren, M., Conley, D.J., Jessen, C., 2006. Rapid Holocene climate changes in the North Atlantic: evidence from lake sediments from the Faroe Islands. Boreas 35, 23–34. https://doi.org/10.1080/03009480500359228.

Arge, S.V., Sveinbjarnardóttir, G., Edwards, K.J., Buckland, P.C., 2005. Viking and medieval settlement in the Faroes: people, place and environment. Hum. Ecol. 33, 597–620. https://doi.org/10.1007/s10745-005-4745-1.

Axford, Y., Briner, J.P., Cooke, C.A., Francis, D.R., Michelutti, N., Miller, G.H., Smol, J.P., Thomas, E.K., Wilson, C.R., Wolfe, A.P., 2009. Recent Changes in a Remote Arctic Lake Are Unique within the Past 200,000 Years 0–3.

Ayache, M., Swingedouw, D., Mary, Y., Eynaud, F., Colin, C., 2018. Multi-centennial variability of the AMOC over the Holocene : a new reconstruction based on multiple proxy-derived SST records. Glob. Planet. Chang. 170, 172–189. https://doi.org/10.1016/j.gloplacha.2018.08.016.

Bakke, J., Lie, Ø., Dahl, S.O., Nesje, A., Bjune, A.E., 2008. Strength and spatial patterns of the Holocene wintertime westerlies in the NE Atlantic region. Glob. Planet. Chang. 60, 28–41. https://doi.org/10.1016/j.gloplacha.2006.07.030.

Baldini, L.M., McDermott, F., Foley, A.M., Baldini, J.U.L., 2008. Spatial variability in the European winter precipitation δ18O-NAO relationship: implications for reconstructing NAO-mode climate variability in the Holocene. Geophys. Res. Lett. 35, L04709. https://doi.org/10.1029/2007GL032027.

Bauch, H.A., Erlenkeuser, H., Fahl, K., Spielhagen, R.F., Weinelt, M.S., Andruleit, H., 1999. Evidence for a steeper Eemian than Holocene sea surface temperature gradient between Arctic and sub-Arctic regions. Palaeogeogr. Palaeoclimatol. Palaeoecol. 145, 95–117.

Behl, R.J., Kennett, J.P., 1996. Brief interstadial events in the Santa Barbara basin, NE Pacific, during the past 60 kyr. Nature. https://doi.org/10.1038/379243a0.

Bennike, O., Hedenäs, L., Lemdahl, G., Wiberg-Larsen, P., 2018. A multiproxy macrofossil record of Eemian palaeoenvironments from Klaksvík, the Faroe Islands. Boreas 47, 106–113. https://doi.org/10.1111/bor.12254.

Bigler, C., Larocque, I., Peglar, S.M., Hall, R.I., 2002. Quantitative multiproxy assessment of long-term patterns of Holocene environmental change from a small lake. Holocene 12, 481–496.

Björck, S., Noe-Nygaard, N., Wolin, J., Houmark-Nielsen, M., Jørgen Hansen, H., Snowball, I., 2000. Eemian Lake development, hydrology and climate: a multi-stratigraphic study of the Hollerup site in Denmark. Quat. Sci. Rev. 19, 509–536. https://doi.org/10.1016/S0277-3791(99)00025-6.

Bjune, A.E., Bakke, J., Nesje, A., Birks, H.J.B., 2005. Holocene mean July temperature and winter precipitation in western Norway inferred from palynological and glaciological lake-sediment proxies. Holocene 15, 177–189.

Blaauw, M., Christen, J.A., 2011. Flexible paleoclimate age-depth models using an autoregressive gamma process. Bayesian Anal. 6, 457–474. https://doi.org/10.1214/11-BA618.

Blockley, S.P.E., Pyne-O'Donnell, S.D.F., Lowe, J.J., Matthews, I.P., Stone, A., Pollard, A.M., Turney, C.S.M., Molyneux, E.G., 2005. A new and less destructive laboratory procedure for the physical separation of distal glass tephra shards from sediments. Quat. Sci. Rev. 24, 1952–1960. https://doi.org/10.1016/J.QUASCIREV.2004.12.008.

Bowen, G.J., 2019. The Online Isotopes in Precipitation Calculator, version 3.1.

Bowen, G.J., Revenaugh, J., 2003. Interpolating the isotopic composition of modern meteoric precipitation. Water Resour. Res. 39, 1–13. https://doi.org/10.1029/2003WR002086.

Bowen, G.J., Wassenaar, L.I., Hobson, K.A., 2005. Global application of stable hydrogen and oxygen isotopes to wildlife forensics. Oecologia 143, 337–348. https://doi.org/10.1007/s00442-004-1813-y.

Boyle, E.A., 1997. Cool tropical temperatures shift the global δ18O-T relationship: an explanation for the ice core δ18O-borehole thermometry conflict? Geophys. Res. Lett. 24, 273–276.

Broecker, W.S., Bond, G., Klas, M., Bonani, G., Wolfi, W., 1990. A salt oscillator in the glacial Atlantic? 1. The concept. Paleoceanography 5, 469–477.

CAPE-Last Interglacial Project Members, 2006. Last Interglacial Arctic warmth confirms polar amplification of climate change. Quat. Sci. Rev. 25, 1383–1400. https://doi.org/10.1016/j.quascirev.2006.01.033.

Cappelen, J., 2018. Weather Observations from Tórshavn, the Faroe Islands 1953-2017.

Capron, E., Govin, A., Stone, E.J., Mulitza, S., Otto-bliesner, B., Rasmussen, T.L., Sime, L.C., Waelbroeck, C., Wolff, E.W., 2014. Temporal and spatial structure of multi-millennial temperature changes at high latitudes during the Last Interglacial. Quat. Sci. Rev. 103, 116–133. https://doi.org/10.1016/j.quascirev.2014.08.018.

Chikaraishi, Y., Naraoka, H., 2007. δ13C and δD relationships among three n-alkyl compound classes (n-alkanoic acid, n-alkane and n-alkanol) of terrestrial higher plants. Org. Geochem. 38, 198–215. https://doi.org/10.1016/j.orggeochem.2006.10.003.

Chikaraishi, Y., Naraoka, H., 2003. Compound-specific δD-δ13C analyses of n-alkanes extracted from terrestrial and aquatic plants. Phytochemistry 63, 361–371. https://doi.org/10.1016/S0031-9422(02)00749-5.

Chikaraishi, Y., Naraoka, H., 2001. Organic hydrogen-carbon isotope signatures of terrestrial higher plants during biosynthesis for distinctive photosynthetic pathways. Geochem. J. 35, 451–458. https://doi.org/10.2343/geochemj.35.451.

Chikaraishi, Y., Naraoka, H., Poulson, S.R., 2004. Carbon and hydrogen isotopic fractionation during lipid biosynthesis in a higher plant (Cryptomeria japonica). Phytochemistry 65, 323–330. https://doi.org/10.1016/j.phytochem.2003.12.003.

Church, M.J., Arge, S.V., Edwards, K.J., Ascough, P.L., Bond, J.M., Cook, G.T., Dockrill, S.J., Dugmore, A.J., McGovern, T.H., NEsbitt, C., Simpson, I.A., 2013. The Vikings were not the first colonizers of the Faroe Islands,. Quat. Sci. Rev. 77, 228–232. https://doi.org/10.1016/j.quascirev.2013.06.011.

Clark, P.U., Pisias, N.G., Stocker, T.F., Weaver, A.J., 2002. The role of thermohaline circulation in abrupt climate change. Nature 415, 863–869. https://doi.org/10.1038/415863a.

CLIMAP Project Members, 1984. The last interglacial ocean. Quat. Res. 21, 123–224. https://doi.org/10.1016/0033-5894(84)90098-X.

Collister, J.W., Rieley, G., Stern, B., Eglinton, G., Fry, B., 1994. Compound-specific δ13C analyses of leaf lipids from plants with differing carbon dioxide metabolisms. Org. Geochem. 21, 619–627. https://doi.org/10.1016/S1352-0237(01)00321-5.

Cortijo, E., Duplessy, J.C., Labeyrie, L., Leclaire, H., Dupart, J., van Weering, T.C.E., 1994. Eemian cooling in the Norwegian Sea and North Atlantic ocean preceding

continental ice-sheet growth. Nat. Clim. Chang. 372, 446–449.
Cranwell, P.A., Eglinton, G., Robinson, N., 1987. Lipids of aquatic organisms as potential contributors to lacustrine sediments–II. Org. Geochem. 11, 513–527.
Dansgaard, W., 1964. Stable isotopes in precipitation. Tellus 16, 436–468. https://doi.org/10.3402/tellusa.v16i4.8993.
De Beaulieu, J.-L., Reille, M., 1992. The last climatic cycle at La Grande pile (Vosges, France): a new pollen profile. Quat. Sci. Rev. 11, 431–438.
Diefendorf, A.F., Freeman, K.H., Wing, S.L., Graham, H.V., 2011. Production of n-alkyl lipids in living plants and implications for the geologic past. Geochem. Cosmochim. Acta 75, 7472–7485. https://doi.org/10.1016/j.gca.2011.09.028.
Dutton, A., Carlson, A.E., Long, A.J., Milne, G.A., Clark, P.U., DeConto, R., Horton, B.P., Rahmstorf, S., Raymo, M.E., 2015. Sea-level rise due to polar ice-sheet mass loss during past warm periods. Science 349 aaaa4019. https://doi.org/10.1126/science.aaa4019.
Eglinton, G., Hamilton, R.J., 1967. Leaf Epicuticular waxes. Science 156, 1322–1335.
Ehleringer, J.R., Hall, A.E., Farquhar, G.D. (Eds.), 1993. Stable Isotopes and Plant Carbon-Water Relations. Academic Press, San Diego.
Elsig, J., Schmitt, J., Leuenberger, D., Schneider, R., Eyer, M., Leuenberger, M., Joos, F., Fischer, H., Stocker, T.F., 2009. Stable isotope constraints on Holocene carbon cycle changes from an Antarctic ice core. Nature 461, 507–510. https://doi.org/10.1038/nature08393.
Farquhar, G.D., O'Leary, M.H., Berry, J.A., 1982. On the relationship between carbon isotope discrimination and the intercellular carbon dioxide concentration in leaves. Aust. J. Plant Physiol. 9, 121–137.
Feakins, S.J., 2013. Pollen-corrected leaf wax D/H reconstructions of northeast African hydrological changes during the late Miocene. Palaeogeogr. Palaeoclimatol. Palaeoecol. 374, 62–71. https://doi.org/10.1016/j.palaeo.2013.01.004.
Feng, X., 1999. Trends in intrinsic water-use efficiency of natural trees for the past 100–200 years: a response to atmospheric CO2 concentration. Geochem. Cosmochim. Acta 63, 1891–1903.
Ficken, K.J., Li, B., Swain, D.L., Eglinton, G., 2000. An n-alkane proxy for the sedimentary input of submerged/floating freshwater aquatic macrophytes. Org. Geochem. 31.
Fronval, T., Jansen, E., Haflidason, H., Sejrup, H.P., 1998. Variability in surface and deep water conditions in the Nordic seas during the last Interglacial period. Quat. Sci. Rev. 17.
Geikie, J., 1881. On the geology of the Færöe islands. Trans. R. Soc. Edinb. 30, 217–269. https://doi.org/10.1017/S0080456800029033.
Gierz, P., Werner, M., Lohmann, G., 2017. Simulating climate and stable water isotopes during the Last Interglacial using a coupled climate-isotope model. J. Adv. Model. Earth Syst. 9, 2027–2045. https://doi.org/10.1002/2017MS001056.
Greve, C., 2001. En Lito-, Bio-, og Kronostratigrafisk Undersøgelse af et Interglacialt, Lacustrint Sediment ved Klaksvík. Geologisk Institut, Kobenhavns Universitet, Bordoy, Nordlige Faeroerne.
Hammarlund, D., Björk, S., Buchardt, B., Israelson, C., Thomsen, C.T., 2003. Rapid hydrological changes during the Holocene revealed by stable isotope records of lacustrine carbonates from Lake Igelsjön, southern Sweden. Quat. Sci. Rev. 22, 353–370.
Hannon, G.E., Bradshaw, R.H.W., 2000. Impacts and timing of the first human settlement on vegetation of the Faroe Islands. Quat. Res. 54, 404–413. https://doi.org/10.1006/qres.2000.2171.
Hannon, G.E., Bradshaw, R.H.W., Bradshaw, E.G., Snowball, I., Wastegård, S., 2005. Climate change and human settlement as drivers of late-Holocene vegetational change in the Faroe Islands. Holocene 5, 639–647.
Hannon, G.E., Bradshaw, R.H.W., Wastegård, S., 2003. Rapid vegetation change during the early Holocene in the Faroe Islands detected in terrestrial and aquatic ecosystems. J. Quat. Sci. 18, 615–619. https://doi.org/10.1002/jqs.783.
Hannon, G.E., Hermanns-Auðardóttir, M., Wastegård, S., 1998. Human impact at Tjørnuvík in the Faroe Islands. FróDskaparrit 46, 215–228.
Hannon, G.E., Rundgren, M., Jessen, C.A., 2010. Dynamic early Holocene vegetation development on the Faroe Islands inferred from high-resolution plant macrofossil and pollen data. Quat. Res. 73, 163–172. https://doi.org/10.1016/j.yqres.2009.11.003.
Hannon, G.E., Wastegård, S., Bradshaw, E., Bradshaw, R.H.W., 2001. Human impact and landscape degradation on the Faroe Islands. Biol. Environ. Proc R. Ir. Acad 101B, 129–139.
Heiri, O., Lotter, A.F., Lemcke, G., 2001. Loss on ignition as a method for estimating organic and carbonate content in sediments: reproducibility and comparability of results. J. Paleolimnol. 25, 101–110.
Holland, A.R., Petsch, S.T., Castaneda, I.S., Wilkie, K.M., Burns, S.J., Brigham-Grette, J., 2013. A biomarker record of Lake El'gygytgyn , Far East Russian Arctic: investigating sources of organic matter and carbon cycling during marine isotope stages 1-3. Clim. Past 9, 243–260. https://doi.org/10.5194/cp-9-243-2013.
Holland, M.M., Bitz, C.M., 2003. Polar amplification of climate change in coupled models. Clim. Dyn. 21, 221–232. https://doi.org/10.1007/s00382-003-0332-6.
Hou, J., Andrea, W.J.D., Huang, Y., 2008. Can sedimentary leaf waxes record D/H ratios of continental precipitation? Field, model, and experimental assessments. Geochem. Cosmochim. Acta 72, 3503–3517. https://doi.org/10.1016/j.gca.2008.04.030.
Jessen, C.A., Rundgren, M., Björck, S., Andresen, C.S., Conley, D.J., 2008. Variability and seasonality of North Atlantic climate during the early Holocene: evidence from Faroe Island lake sediments. Holocene 18, 851–860.
Johansen, J., 1985. Studies in the vegetational history of the Faroe and Shetland islands. Ann. Soc. Sci. Færoensis Suppl. 11.
Johansen, J., 1981. Vegetational development in the Faroes from 10,000 BP to the present. Årbog-Dansmarks Geol. undersøgelse 111–136.
Johansen, J., 1975. Pollen diagrams from the Shetland and Faroe Islands. New Phytol. 75, 369–387.
Jørgensen, G., Rasmussen, J., 1986. Glacial Striae, Roches Moutonnées, and Ice Movements in the Faroe Islands.
Jouzel, J., Mason-Delmotte, V., Cattani, O., Dreyfus, G., Falourd, S., Hoffmann, G., Minster, B., Nouet, J., Barnola, J.M., Chappellaz, J., Fischer, H., Gallet, J.C., Johnsen, S., Leuenberger, M., Loulergue, L., Luethi, D., Oerter, H., Parrenin, F., Raisbeck, G., Raynaud, D., Schilt, A., Schwander, J., Selmo, E., Souchez, R., Spahni, R., Stauffer, B., Steffensen, J.P., Stenni, B., Stocker, T.F., Tison, J.L., Werner, M., Wolff, E.W., 2007. Orbital and millennial Antarctic climate variability over the past 800,000 years. Science 317, 793–796.
Kahmen, A., Schefuß, E., Sachse, D., 2013. Leaf water deuterium enrichment shapes leaf wax n-alkane δD values of angiosperm plants II: observational evidence and global implications. Geochem. Cosmochim. Acta 111, 39–49. https://doi.org/10.1016/j.gca.2012.09.003.
Kaspar, F., Ku, N., Cubasch, U., Litt, T., 2005. A model-data comparison of European temperatures in the Eemian interglacial. Geophys. Res. Lett. 32, 1–5. https://doi.org/10.1029/2005GL022456.
Kühl, N., Litt, T., 2003. Quantitative time series reconstruction of Eemian temperature at three European sites using pollen data. Veg. Hist. Archaeobotany 12, 205–214. https://doi.org/10.1007/s00334-003-0019-2.
Kukla, G.J., Bender, M.L.B., de Beaulieu, J.-L., Bond, G., Broecker, W.S., Cleveringa, P., Gavin, J.E., Herbert, T.D., Imbrie, J., Jouzel, J., Keigwin, L.D., Knudsen, K.-L., McManus, J.F., Merkt, J., Muhs, D.R., Muller, H., Poore, R.Z., Porter, S.C., Seret, G., Shackleton, N.J., Turner, C., Tzedakis, P.C., Winograd, I.J., 2002. Last interglacial climates. Quat. Res. 58, 2–13. https://doi.org/10.1006/qres.2001.2316.
Kylander, M.E., Lind, E.M., Wastegård, S., Löwemark, L., 2012. Recommendations for using XRF core scanning as a tool in tephrochronology. Holocene. https://doi.org/10.1177/0959683611423688.
Langdon, P.G., Leng, M.J., Holmes, N., Caseldine, C.J., 2010. Lacustrine evidence of early-Holocene environmental change in northern Iceland: a multiproxy palaeoecology and stable isotope study. Holocene 20, 205–214. https://doi.org/10.1177/0959683609354301.
Lawson, I.T., Church, M.J., Edwards, K.J., Cook, G.T., Dugmore, A.J., 2007. Peat initiation in the Faroe Islands: climate change, pedogenesis or human impact? Earth Environ. Sci. Trans. R. Soc. Edinburgh 98, 15–28. https://doi.org/10.1017/S1755691007000035.
Lawson, I.T., Church, M.J., McGovern, T.H., Arge, S.V., Woollet, J., Edwards, K.J., Gathorne-Hardy, F.J., Dugmore, A.J., Cook, G., Mairs, K.A., Thomson, A.M., Sveinbjarnardóttir, G., 2005. Historical ecology on Sandoy, Faroe Islands: palaeoenvironmental and archaeological perspectives. Hum. Ecol. 33, 651–684. https://doi.org/10.1007/s10745-005-7681-1.
Lawson, I.T., Edwards, K.J., Church, M.J., Newton, A.J., Cook, G.T., Gathorne-hardy, F.J., Dugmore, A.J., 2008. Human impact on an island ecosystem: pollen data from Sandoy, Faroe Islands. J. Biogeogr. 35, 1130–1152. https://doi.org/10.1111/j.1365-2699.2007.01838.x.
LeGrande, A.N., Schmidt, G.A., 2008. Ensemble, water isotope-enabled, coupled general circulation modeling insights into the 8.2 ka event. Paleoceanography 23, PA3207. https://doi.org/10.1029/2008PA001610.
Lohne, Ø.S., Mangerud, J., Birks, H.H., 2013. Precise 14C ages of the Vedde and Saksunarvatn ashes and the Younger Dryas boundaries from western Norway and their comparison with the Greenland Ice Core (GICC05) chronology. J. Quat. Sci. 28, 490–500. https://doi.org/10.1002/jqs.2640.
Lourantou, A., Chappellaz, J., Barnola, J.-M., Masson-Delmotte, V., Raynaud, D., 2010. Changes in atmospheric CO2 and its carbon isotopic ratio during the penultimate deglaciation. Quat. Sci. Rev. 29, 1983–1992. https://doi.org/10.1016/j.quascirev.2010.05.002.
Maffei, M., 1996. Chemotaxonomic significance of leaf wax alkanes in the gramineae. Biochem. Syst. Ecol. 24, 53–64. https://doi.org/10.1016/0305-1978(95)00102-6.
Manabe, S., Stouffer, R.J., 1980. Sensitivity of a global climate model to an increase of CO2 concentration in the atmosphere. J. Geophys. Res. 85, 5529–5554.
Mangerud, J., Sønstegaard, E., Sejrup, H.-P., Haldorsen, S., 1981. A continuous Eemian-Early Weichselian sequence containing pollen and marine fossils at Fjøsanger, western Norway. Boreas 10, 137–208.
Manthé, S., 1998. Variabilité de la circulation thermohaline glaciaire et interglaciaire en Atlantique Nord tracée par les foraminifères planctoniques et la microfaune benthique. Université de Bordeaux, France.
Marcott, S.A., Shakun, J.D., Clark, P.U., Mix, A.C., 2013. A reconstruction of regional and global temperature for the past 11,300 years. Science 339, 1198–1202.
Marsicek, J., Shuman, B.N., Bartlein, P.J., Shafer, S.L., Brewer, S., 2018. Reconciling divergent trends and millennial variations in Holocene temperatures. Nature 554, 92–96. https://doi.org/10.1038/nature25464.
McFarlin, J.M., Axford, Y., Osburn, M.R., Kelly, M.A., Osterberg, E.C., Farnsworth, L.B., 2018. Pronounced summer warming in northwest Greenland during the Holocene and last interglacial. Proc. Natl. Acad. Sci. 1–6. https://doi.org/10.1073/pnas.1720420115.
McKay, N.P., Overpeck, J.T., Otto-Bliesner, B.L., 2011. The role of ocean thermal expansion in Last Interglacial sea level rise. Geophys. Res. Lett. 38, L14605. https://doi.org/10.1029/2011GL048280.
Meyers, P.A., Teranes, J.L., 2001. Sediment organic matter. In: Last, W.M., Smol, J.P. (Eds.), Tracking Environmental Change Volume 2: Physical and Geochemical Methods. Kluwer Academic Publishers, Dordrecht, The Netherlands, pp. 239–269.

Monnin, E., Steig, E.J., Siegenthaler, U., Kawamura, K., Schwander, J., Stauffer, B., Stocker, T.F., Morse, D.L., Barnola, J.-M., Bellier, B., Raynaud, D., Fischer, H., 2004. Evidence for substantial accumulation rate variability in Antarctica during the Holocene, through synchronization of CO2in the Taylor Dome, Dome C and DML ice cores. Earth Planet. Sci. Lett. 224, 45–54. https://doi.org/10.1016/j.epsl.2004.05.007.

NEEM Community Members, 2013. Eemian interglacial reconstructed from a Greenland folded ice core. Nature 493, 489–494. https://doi.org/10.1038/nature11789.

Nichols, J., Booth, R.K., Jackson, S.T., Pendall, E.G., Huang, Y., 2010. Differential hydrogen isotopic ratios of Sphagnum and vascular plant biomarkers in ombrotrophic peatlands as a quantitative proxy for precipitation—evaporation balance. Geochem. Cosmochim. Acta 74, 1407–1416. https://doi.org/10.1016/j.gca.2009.11.012.

Olsen, J., Björck, S., Leng, M.J., Gudmundsdóttir, E.R., Odgaard, B.V., Lutz, C.M., Kendrick, C.P., Andersen, T.J., Seidenkrantz, M.-S., 2010. Lacustrine evidence of Holocene environmental change from three Faroese lakes: a multiproxy XRF and stable isotope study. Quat. Sci. Rev. 29, 2764–2780. https://doi.org/10.1016/j.quascirev.2010.06.029.

Oppo, D.W., McManus, J.F., Cullen, J.L., 2006. Evolution and demise of the last interglacial warmth in the subpolar North Atlantic. Quat. Sci. Rev. 25, 3268–3277. https://doi.org/10.1016/j.quascirev.2006.07.006.

Otto-Bliesner, B.L., Rosenbloom, N., Stone, E.J., Mckay, N.P., Lunt, D.J., Brady, E.C., Overpeck, J.T., 2013. How warm was the last interglacial? New model–data comparisons. Philos. Trans. R. Soc. 371, 20130097.

Peterson, L.C., Haug, G.H., Hughen, K.A., Röhl, U., 2000. Tropical Atlantic during the last glacial rapid changes in the hydrologic cycle of the tropical Atlantic during the last glacial. Science 290, 1947–1951. https://doi.org/10.1126/science.290.5498.1947.

Pfeiffer, M., Lohmann, G., 2016. Greenland Ice Sheet influence on Last Interglacial climate: global sensitivity studies performed with an atmosphere-ocean general circulation model. Clim. Past 12, 1313–1338. https://doi.org/10.5194/cp-12-1313-2016.

Pierrehumbert, R.T., 1999. Huascaran δ18O as an indicator of tropical climate during the Last Glacial Maximum. Geophys. Res. Lett. 26, 1345–1348.

Polissar, P.J., D'Andrea, W.J., 2014. Uncertainty in paleohydrologic reconstructions from molecular δD values. Geochem. Cosmochim. Acta 129, 146–156. https://doi.org/10.1016/j.gca.2013.12.021.

Polissar, P.J., Freeman, K.H., 2010. Effects of aridity and vegetation on plant-wax δD in modern lake sediments. Geochem. Cosmochim. Acta 74, 5785–5797. https://doi.org/10.1016/j.gca.2010.06.018.

Poynter, J., Eglinton, G., 1990. Molecular composition of three sediments from Hole 717C: the Bengal fan, proceedings of the ocean drilling program. Sci. Results 116. In: https://doi.org/10.2973/odp.proc.sr.116.151.1990.

Rach, O., Kahmen, A., Brauer, A., Sachse, D., 2017. A dual-biomarker approach for quantification of changes in relative humidity from sedimentary lipid D/H ratios. Clim. Past 13, 741–757.

Rasmussen, J., 1972. Morena a Bordoyarvık, som bendir aeitt millumbil ı glersetingini har norduri. Frodskaparrit 20, 54–70.

Rasmussen, J., Noe-Nygaard, A., 1970. Geology of the Faeroe Islands (Pre-quaternary) (Copenhagen).

Rasmussen, T.L., Thomsen, E., 2010. Holocene temperature and salinity variability of the Atlantic Water inflow to the Nordic seas. Holocene 20, 1223–1234. https://doi.org/10.1177/0959683610371996.

Rasmussen, T.L., Thomsen, E., Kuijpers, A., Wastegård, S., 2003. Late warming and early cooling of the sea surface in the Nordic seas during MIS 5e (Eemian Interglacial). Quat. Sci. Rev. 22, 809–821. https://doi.org/10.1016/S0277-3791(02)00254-8.

Reimer, P.J., Bard, E., Bayliss, A., Beck, J.W., Blackwell, P.G., Ramsey, C.B., Buck, C.E., Cheng, H., Edwards, R.L., Friedrich, M., Grootes, P.M., Guilderson, T.P., Haflidason, H., Hajdas, I., Hatté, C., Heaton, T.J., Hoffmann, D.L., Hogg, A.G., Hughen, K.A., Kaiser, K.F., Kromer, B., Manning, S.W., Niu, M., Reimer, R.W., Richards, D.A., Scott, E.M., Southon, J.R., Staff, R.A., Turney, C.S.M., van der Plicht, J., 2013. IntCal13 and Marine 13 radiocarbon age calibration curves 0–50,000 Years cal BP. Radiocarbon 55, 1869–1887. https://doi.org/10.2458/azu_js_rc.55.16947.

Sachse, D., Billault, I., Bowen, G.J., Chikaraishi, Y., Dawson, T.E., Feakins, S.J., Freeman, K.H., Magill, C.R., McInerney, F.A., van der Meer, M.T.J., Polissar, P., Robins, R.J., Sachs, J.P., Schmidt, H.-L., Sessions, A.L., White, J.W.C., West, J.B., Kahmen, A., 2012. Molecular paleohydrology: interpreting the hydrogen-isotopic composition of lipid biomarkers from photosynthesizing organisms. Annu. Rev. Earth Planet Sci. 40, 221–249. https://doi.org/10.1146/annurev-earth-042711-105535.

Sachse, D., Radke, J., Gleixner, G., 2004. Hydrogen isotope ratios of recent lacustrine sedimentary n-alkanes record modern climate variability. Geochem. Cosmochim. Acta 68, 4877–4889. https://doi.org/10.1016/j.gca.2004.06.004.

Salonen, J.S., Helmens, K.F., Brendryen, J., Kuosmanen, N., Väliranta, M., Goring, S., Korpela, M., Kylander, M., Philip, A., Plikk, A., Renssen, H., Luoto, M., 2018. Abrupt high-latitude climate events and decoupled seasonal trends during the Eemian. Nat. Commun. 9, 2851. https://doi.org/10.1038/s41467-018-05314-1.

Sauer, P.E., Eglinton, T.I., Hayes, J.M., Schimmelmann, A., Sessions, A.L., 2001. Compound-specific D/H ratios of lipid biomarkers from sediments as a proxy for environmental and climatic conditions. Geochem. Cosmochim. Acta 65, 213–222.

Scheidegger, Y., Saurer, M., Bahn, M., Siegwolf, R., 2000. Linking stable oxygen and carbon isotopes with stomatal conductance and photosynthetic capacity: a conceptual model. Oecologia 125, 350–357. https://doi.org/10.1007/s004420000466.

Seibt, U., Rajabi, A., Griffiths, H., Berry, J.A., 2008. Carbon isotopes and water use efficiency: sense and sensitivity. Oecologia 155, 441–454. https://doi.org/10.1007/s00442-007-0932-7.

Seki, O., Meyers, P.A., Yamamoto, S., Kawamura, K., Nakatsuka, T., Zhou, W., Zheng, Y., 2011. Plant-wax hydrogen isotopic evidence for postglacial variations in delivery of precipitation in the monsoon domain of China. Geology 39, 875–878. https://doi.org/10.1130/G32117.1.

Seppa, H., Birks, H.J.B., 2001. July mean temperature and annual precipitation trends during the Holocene in the Fennoscandian tree-line area: pollen-based climate reconstructions. Holocene 11, 527–539.

Serreze, M.C., Francis, J.A., 2006. The arctic amplification debate. Clim. Change 76, 241–264. https://doi.org/10.1007/s10584-005-9017-y.

Shackleton, N.J., Sánchez-Goñi, M.F., Pailler, D., Lancelot, Y., 2003. Marine isotope substage 5e and the Eemian interglacial. Glob. Planet. Chang. 36, 151–155. https://doi.org/10.1016/S0921-8181(02)00181-9.

Sundqvist, H.S., Kaufman, D.S., McKay, N.P., Balascio, N.L., Briner, J.P., Cwynar, L.C., Sejrup, H.P., Seppä, H., Subetto, D.A., Andrews, J.T., Axford, Y., Bakke, J., Birks, H.J.B., Brooks, S.J., de Vernal, A., Jennings, A.E., Ljungqvist, F.C., Rühland, K.M., Saenger, C., Smol, J.P., Viau, A.E., 2014. Arctic Holocene proxy climate database—New approaches to assessing geochronological accuracy and encoding climate variables. Clim. Past 10, 1605–1631. https://doi.org/10.5194/cp-10-1605-2014.

Thornalley, D.J.R., Blaschek, M., Davies, F.J., Praetorius, S., Oppo, D.W., McManus, J.F., Hall, I.R., Kleiven, H., Renssen, H., McCave, I.N., 2013. Long-term variations in Iceland-Scotland overflow strength during the Holocene. Clim. Past 9, 2073–2084. https://doi.org/10.5194/cp-9-2073-2013.

Turney, C.S.M., Harkness, D.D., Lowe, J.J., 1997. The use of microtephra horizons to correlate Late-glacial lake sediment successions in Scotland. J. Quat. Sci. 12, 525–533.

Turney, C.S.M., Jones, R.T., 2010. Does the Agulhas Current amplify global temperatures during super-interglacials? J. Quat. Sci. 25, 839–843. https://doi.org/10.1002/jqs.1423.

van Bree, L.G.J., Peterse, F., van der Meer, M.T.J., Middelburg, J.J., Negash, A.M.D., De Crop, W., Cocquyt, C., Wieringa, J.J., Verschuren, D., Sinninghe Damsté, J.S., 2018. Seasonal variability in the abundance and stable carbon-isotopic composition of lipid biomarkers in suspended particulate matter from a stratified equatorial lake (Lake Chala, Kenya/Tanzania): implications for the sedimentary record. Quat. Sci. Rev. 192, 208–224. https://doi.org/10.1016/j.quascirev.2018.05.023.

Van Nieuwenhove, N., Bauch, H.A., Eynaud, F., Kandiano, E., Cortijo, E., Turon, J., 2011. Evidence for delayed poleward expansion of North Atlantic surface waters during the last interglacial (MIS 5e). Quat. Sci. Rev. 30, 934–946. https://doi.org/10.1016/j.quascirev.2011.01.013.

Wang, Y.J., Cheng, H., Edwards, R.L., An, Z.S., Wu, J.Y., Shen, C.-C., Dorale, J.A., 2001. A high-resolution absolute-dated late pleistocene monsoon record from Hulu Cave , China. Science 294, 2345–2348. https://doi.org/10.1126/science.1064618.

Wastegård, S., Björck, S., Grauert, M., Hannon, G.E., 2001. The Mjáuvøtn tephra and other Holocene tephra horizons from the Faroe Islands: a link between the Icelandic source region, the Nordic Seas, and the European continent. Holocene 11, 101–109. https://doi.org/10.1191/095968301668079904.

Wastegård, S., Björck, S., Greve, C., Rasmussen, T.L., 2005. A tephra-based correlation between the Faroe Islands and the Norwegian Sea raises questions about chronological relationships during the last interglacial. Terra. Nova 17, 7–12. https://doi.org/10.1111/j.1365-3121.2004.00578.x.

Wastegård, S., Gudmundsdottir, E.R., Lind, E.M., Timms, R.G.O., Bjorck, S., Hannon, G.E., Olsen, J., Rundgren, M., 2018. Towards a Holocene tephrochronology for the Faroe Islands, North Atlantic. Quat. Sci. Rev. 195, 195–214. https://doi.org/10.1016/j.quascirev.2018.07.024.

Wastegård, S., Rundgren, M., Schoning, K., Andersson, S., Björck, S., Borgmark, A., Possnert, G., 2008. Age, geochemistry and distribution of the mid-Holocene Hekla-S/Kebister tephra. Holocene 18, 539–549. https://doi.org/10.1177/0959683608089208.

Zagwijn, W.H., 1996. An analysis of Eemian climate in western and central Europe. Quat. Sci. Rev. 15, 451–469. https://doi.org/10.1016/0277-3791(96)00011-X.

Zhang, Z., Sachs, J.P., 2007. Hydrogen isotope fractionation in freshwater algae: I. Variations among lipids and species. Org. Geochem. 38, 582–608. https://doi.org/10.1016/j.orggeochem.2006.12.004.

Ziegler, H., 1989. Hydrogen isotope fractionation in plant tissues. In: Rundel, P.W., Ehleringer, J.R., Nagy, K.A. (Eds.), Stable Isotopes in Ecological Research. Springer-Verlag, New York, pp. 105–123.